UCRL-6578
Nuclear Explosions—
Peaceful Applications, UC-35
TID-4500 (16th Ed.)

UNIVERSITY OF CALIFORNIA
Lawrence Radiation Laboratory
Livermore, California

Contract No. W-7405-eng-48

ON CRATERING

A Brief History, Analysis, and Theory of Cratering

Milo D. Nordyke

August 22, 1961

DISCLAIMER

CONTENTS

CONTENTS (Cont d.)

ON CRATERING

A Brief History, Analysis, and Theory of Cratering

Milo D. Nordyke

Lawrence Radiation Laboratory, University of California
Livermore, California

August 22, 1961

ABSTRACT

Cratering is a subject that has been studied by many investigators for many years for many purposes. These purposes range from experimental studies of physical properties to large scale excavations using explosive charges of kiloton size. In the past ten years considerable effort has been devoted to cratering experiments for the purposes of determining the effects of cratering by nuclear explosions, with recent accent on Plowshare applications. From the large amount of data available for craters in alluvium it has been possible to establish very reliable relationships between charge size, depth of burst, crater radii, and crater depths. In addition it has been possible to construct a preliminary theory of the mechanics of explosive crater formation. In this report the available experimental data for nuclear and high explosive craters are reviewed, with particular emphasis on the data for desert alluvium, and the pertinent relationships are derived. A theory of the important cratering mechanisms, which has been evolved on the basis of these data and data from other sources, is outlined.

ON CRATERING

A Brief History, Analysis, and Theory of Cratering

Milo D. Nordyke

Lawrence Radiation Laboratory, University of California
Livermore, California

CHAPTER I. INTRODUCTION

General

Cratering is a subject that has been studied by many investigators for many years. The first interest in man-made craters probably dates from the invention of gunpowder and stemmed from "scientific" curiosity. Over the years this motivation has been supplemented by many others directed toward practical utilization of gunpowder and other much more potent energy sources. In recent years these purposes have included (1) determination of physical properties and characteristics of rocks and soils as well as of the explosive themselves, (2) understanding such phenomena as impact craters, and hence modeling of meteorite and lunar craters, (3) study of the mechanics of cratering, (4) modeling of effects of nuclear craters, and (5) useful large-scale excavation projects.

Use of high explosives (H. E.) to characterize rock types has been practiced in the mining industry for a long time. This work ranges from determining the maximum amount of rock breakage per unit charge to investigations related to the best charge location for timed demolition. In recent years laboratory and field studies by scientists have used cratering to determine physical constants, such as dynamic tensil strengths,[1] for a wide variety of rocks.

Experiments with impact craters are relatively recent, particularly at the very high velocities made possible through the development of hypervelocity gas guns.[2] These impact cratering experiments along with data from large chemical and nuclear explosion craters have been used by scientists in attempts to explain the origin of lunar and terrestrial meteor craters.[3,4,5] These efforts have been quite successful and have led to a renewed general scientific interest in cratering.

All of the above work entails some reference to the mechanics of crater information. In addition, a few investigators have conducted experiments

specifically directed toward exploring one or another of the mechanisms involved in cratering. However, the author knows of no study covering all mechanisms that has been made and, to date, no complete theory of cratering has been proposed.

Use of craters and cratering for excavation and construction purposes has been practiced extensively in the Soviet Union with charge sizes as large as 9000 tons of chemical explosive.[6,7] Much of this work has been for the purpose of strip mining, overburden removal, and river diversion through construction of dams and canals. The largest such projects in North America using high explosives to break and eject large quantities of rock include such projects as Ripple Rock[8] in Canada, which used about 1000 tons of ammonium nitrate to remove an underwater hazard, and the Promontory Point quarry blasts in Utah.[9]

In the past 10 years considerable effort has been devoted to determining the effects of cratering by nuclear weapons. This effort included a few nuclear craters and a large number of high explosive craters. To simulate the effects of bomb-delivered nuclear weapons all of this work was done with very shallow depths of burst. Since the use of nuclear explosives for large-scale excavation projects requires large depths of burial, to optimize crater dimensions and suppress radioactivity release and air blast, these data have been extended in the past several years to large depths of burst by high-explosive cratering programs sponsored by the Plowshare Program of the AEC. In addition, Plowshare has sponsored programs for investigating the effects of large-yield chemical explosives, linear charge configurations,[10] and cratering in a hard rock medium.[11]

The author's interest in craters stems largely from the latter three fields of interest, namely the mechanics of cratering, the use of explosives for large-scale excavation projects, and in particular, the use of nuclear explosives for cratering. From the large amount of data available for craters in alluvium it has been possible to establish very good relationships between charge size, depth of burst, crater radii, and crater depths. For the case of nuclear craters it has also been possible to derive a relation between the amount of radioactivity released, the air blast generated, and the depth of burst. In addition, it has been possible to construct a preliminary theory of the mechanics of explosive crater formation. In this report the available experimental data for nuclear and high explosive

craters in alluvium are reviewed and the relationships derived are given. The cratering theory that has been evolved on the basis of these data and from other sources is then outlined.

Nuclear Excavation

The use of nuclear craters for useful purposes such as harbors, canals, strip mining, and similar large-scale excavation projects has been termed "nuclear excavation" by the Plowshare Program of industrial application of nuclear explosives. The use of nuclear explosives on excavation projects differs significantly from the use of conventional chemical explosives. Whereas chemical explosives are used to crush and break rock which is subsequently removed with conventional earth-moving equipment, nuclear explosives produce craters so large that no postdetonation removal of material is necessary. A 1-megaton nuclear explosive costing about $1 million will remove about 100 million cubic yards, for an earth-moving cost of about a penny a cubic yard. This can be compared to a cost by conventional methods ranging from 50 cents to $5 per cubic yard. Of course, on many excavation projects it is not possible to exactly compare costs per cubic yard in this way since nuclear excavation generally removes considerably more material than would be blasted and dug out by conventional methods.

The safety problems associated with nuclear cratering detonations have been carefully considered, and the conclusion is that nuclear excavation projects can be performed in a manner that is completely safe.[12,13] As will be shown, proper location of the explosive results in more than 90% of the activity being retained underground. Close-in air blast can similarly be attenuated by a large factor. Seismic disturbance is not believed to be a limiting factor. Selection of proper meteorological conditions at shot times will result in safe conduct of the operation. Those factors that relate to the safety of nuclear excavation are being studied concurrently with the technical aspects of cratering itself.

Definitions and Background

For the purpose of this paper, definitions of several of the terms to be used should be made. Unfortunately, there is no uniform terminology in the field of elastoplastic behavior, and each writer is forced to define his

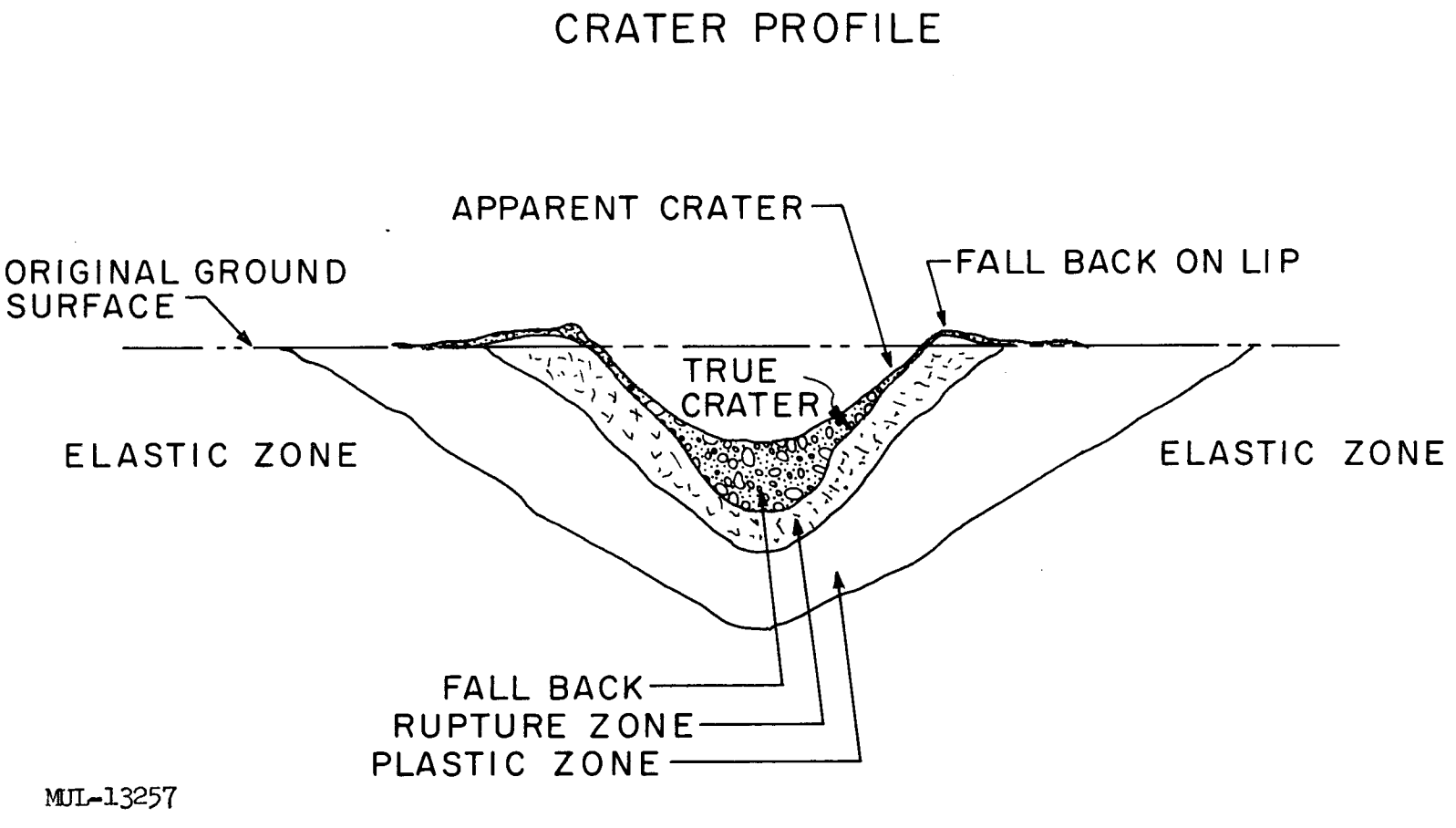

Fig. 1. Schematic drawing of a typical crater.

own terms for his purposes. This situation, of course, arises to a great extent because of the tremendous range of properties of materials causing definitions that are adequate for one material to be unsuitable for another.

Figure 1 is a schematic drawing of a typical crater cross section showing the pertinent parameters. The apparent crater is defined as the crater that is visible on the surface, the dimensions being measured with respect to the original ground level. The true crater is defined as the boundary between the loose, broken fallback material and the underlying material that has been crushed and fractured but has not experienced significant vertical displacement. The products of the explosion are widely dispersed throughout the fallback material that rests in the true crater after the explosion.

The rupture zone is perhaps the most difficult to define, particularly with regard to differentiating it from the plastic zone. There is, of course, a gradual transition from one zone to the other. Near the true crater interface large amounts of fracturing and crushing by shear failure and gross displacements by faulting and underthrusting are generally seen. Their severity decreases as one goes farther into the rupture zone until near the rupture zone-plastic zone interface only small-scale shear failures (of the order of an inch) are found. This zone gradually shades into the plastic zone in which there are small uniform permanent displacements which decrease to infinitesimal values as one goes into the elastic zone.

The extent of these zones is very dependent on the medium, varying widely as one goes from a soft medium like alluvium to a hard medium like basalt. The definitions given here have been derived principally for soft materials such as alluvium, and there would have to be some redefinition of these terms for a discussion of cratering in hard rock.

To correlate results from cratering explosions with different yields or charge weights, dimensional analysis suggests a basic scaling law in which dimensions are proportional to $W^{1/3}$, where W is the weight of the explosive (in pounds or kilotons). Distances or times associated with explosions of different charge weights can be put on the same scale for comparison purposes by dividing them by $W^{1/3}$. Quantities like pressures and velocities are constant. Thus, at the same scaled distance and the same scaled time, we should have the same actual pressure in the shock

wave and the same actual particle velocities. However, the analysis that leads to $W^{1/3}$ scaling ignores the action of several factors such as gravity and the strength or internal frictional forces of the medium. While the extent of these forces is difficult to evaluate, one can show[14] that their effect would be to lower the exponent and lead toward $W^{1/4}$ scaling. Early work by Vaile[15] and more recent work by Chabai[16] and others[17] indicate that $W^{1/3.4}$ scaling would be more correct than $W^{1/3}$. In the analysis portion of this report it will be shown that $W^{1/3.4}$ scaling agrees quite well with the data from the recent 40,000-lb craters and the 1-million-lb Scooter crater in desert alluvium.

It should be noted at this point that the forces which lead toward $W^{1/4}$ scaling are most important for apparent crater dimensions and do not as strongly influence true crater dimensions. It is recommended that $W^{1/3}$ scaling be used for all effects except when discussing apparent crater phenomena.

The data from cratering experiments that are most useful to excavation projects are the dimensions of the apparent crater as a function of the scaled depth of burst (i.e., depth of burial), of the explosive charge. As the explosive is buried successively deeper, the crater dimensions increase, go through a maximum, and ultimately fall to zero when camouflet conditions are reached. Such a behavior is more or less typical of all media, although the maxima have different values and occur at different depths of burst. In addition, it should be noted that the scatter of the data points is quite large, particularly at depths of burst deeper than optimum, due to variations in the physical properties of the rock.

CHAPTER II. NUCLEAR CRATERING EXPERIENCE

Nuclear Craters

Four nuclear explosives have been detonated at the Nevada Test Site (NTS) under conditions which resulted in the creation of large craters. Three of these were fired for the purposes of nuclear weapons effects studies and hence were at rather shallow depths of burst, much shallower than proposed Plowshare applications. All three of these detonations occurred in the valley alluvial fill of Area 10 at NTS, a medium characterized as a loose, sand-gravel mixture with a density of approximately 1.5-1.7 and a water content, at depth, of about 10%. The fourth nuclear crater, Neptune, was made in the bedded tuff of the Rainier mesa at NTS. This medium is a weakly cemented volcanic ash in which all the deep underground nuclear explosions (Rainier, Blanca, Logan, et al.) have been fired.

In Table I are given the apparent crater dimensions, measured with respect to the original ground level for these four nuclear craters. In Fig. 2 the crater profiles have all been scaled to 1 kiloton for comparison purposes. Some discussion of each crater will be useful.

Table I. Summary of nuclear cratering data from the Nevada Test Site.

				Dimensions of Apparent Crater				
Shot Name	Medium	Yield (kt)	Depth of Burst (ft)	Radius, R(ft)	Depth, D(ft)	Volume (yd^3)	R D	Lip Height (ft)
Jangle S	Alluvium	1.2±0.1	-3.5*	45	21	1650	2.15	-
Jangle U	Alluvium	1.2±0.1	17	130	53	3.7×10^4	2.45	8
Teapot ESS	Alluvium	1.2±0.1	67	146	90	9.6×10^4	1.62	19
Neptune**	Tuff	0.115±0.015	100	100	35	2.2×10^4	2.86	-

*Detonated 3.5 ft above surface.
**Neptune was detonated 100 ft beneath a 30° slope.

Jangle S. The Jangle S event was a 1.2-kt nuclear explosive detonated 3.5 feet above the surface of the ground in late 1951. As can be seen from Fig. 2, the crater formed was very small and contained essentially no loose fallback material. The crater and lip were formed almost entirely by plastic deformation of the ground by the action of the fireball. An additional reason for the small size of the crater is that, for a nuclear device, about

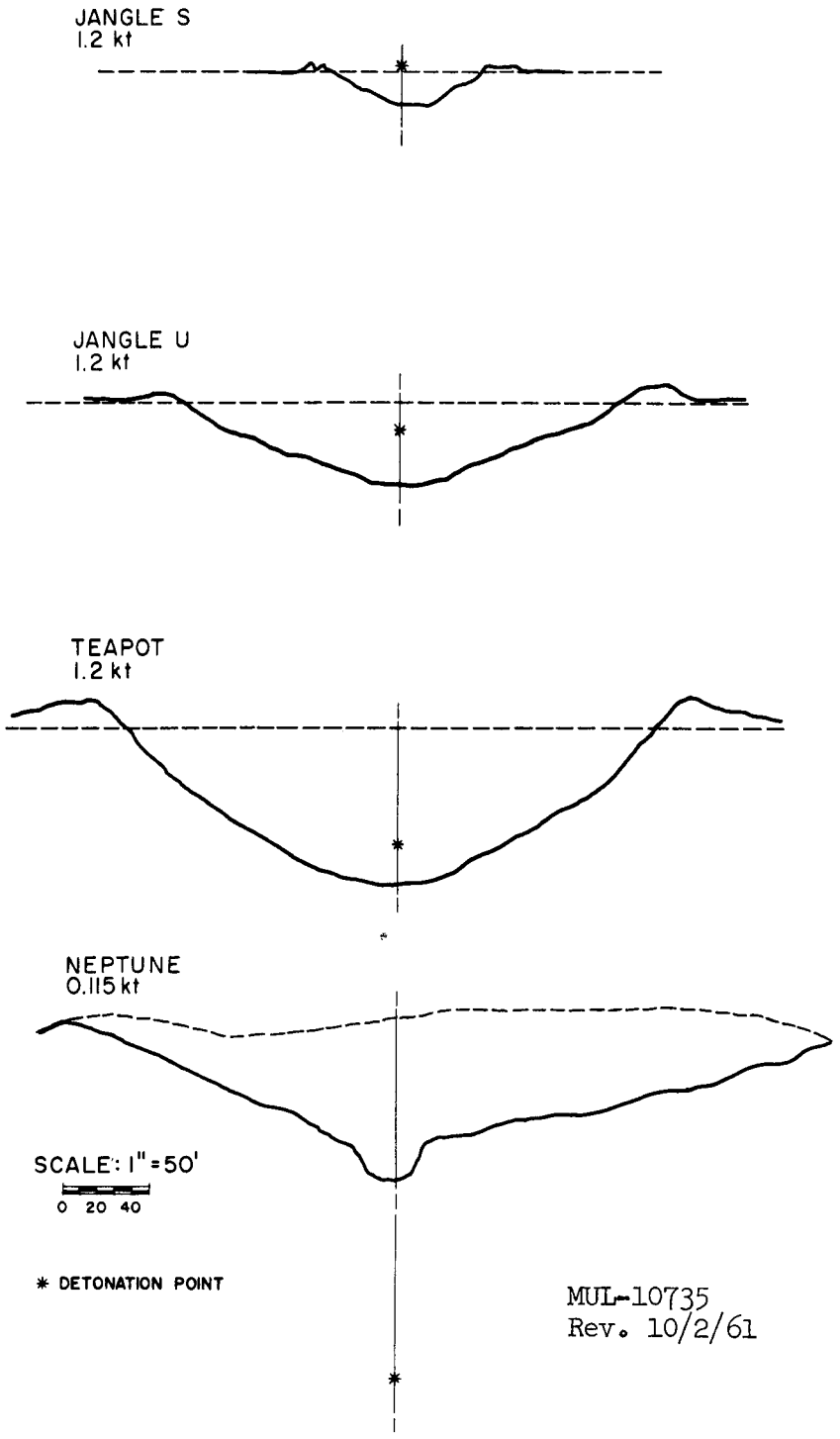

Fig. 2. Nuclear crater profiles.

a third of the released energy is in the form of thermal and x-ray radiation, which is lost immediately for a surface burst. For a subsurface burst, this energy is used for vaporization and melting of the medium surrounding the device, so that a portion of its energy is available for later utilization.

Jangle U. The 1.2-kt nuclear device used for the Jangle U event, also detonated in late 1951, was placed in a concrete-lined room, 10 × 10 × 8 feet high. The hole from the top of the room to the surface was stemmed with a sandbag plug. The center of the device was 17 feet below the surface of the ground. The crater resulting from this explosion was considerably larger than the Jangle S crater but still much smaller than the maximum possible crater for a 1.2-kt explosion. A brief flash of the fireball was observed, but for a much shorter length of time than for Jangle S. A dense dust cloud rose to a height of about 6000 feet and a base surge was formed which spread out radially to a distance of about 1 mile. Almost all the radioactivity escaped to the atmosphere and was deposited on the surface within 10 miles.

Teapot ESS. Teapot ESS was fired during Operation Teapot in March 1955 at a site very near the Jangle U crater. The 1.2-kt device was located 67 feet below the surface at the bottom of a 10-foot-diameter hole. A larger 30-foot hole was provided for personnel access prior to the explosion. The device was packed closely with sandbag plugs and both holes were filled with loose, alluvial material before the detonation. A brief flash of very short duration was also observed on detonation of this device. Again a base surge about 1 mile in radius was formed. Survey of the total radioactivity after the explosion revealed that about 70% was released in a manner similar to that of Jangle U. The crater produced had dimensions considerably larger than Jangle U's because of the large depth of burst, which gave much better coupling of the explosion energy to the ground. However, these dimensions are still much smaller than the maximum possible dimensions based on high-explosive experimental data at large depth of burst.

An extensive program to delineate the true crater was undertaken for the Teapot event.[18] Twenty-one colored sand columns were emplaced along a diameter to depths ranging from 50 to 200 feet as shown in Fig. 3. Postshot excavation of a trench through the crater along this diameter revealed the situation shown in Fig. 4. The true crater and rupture zones were fairly well defined by these columns. Of particular interest were the final locations

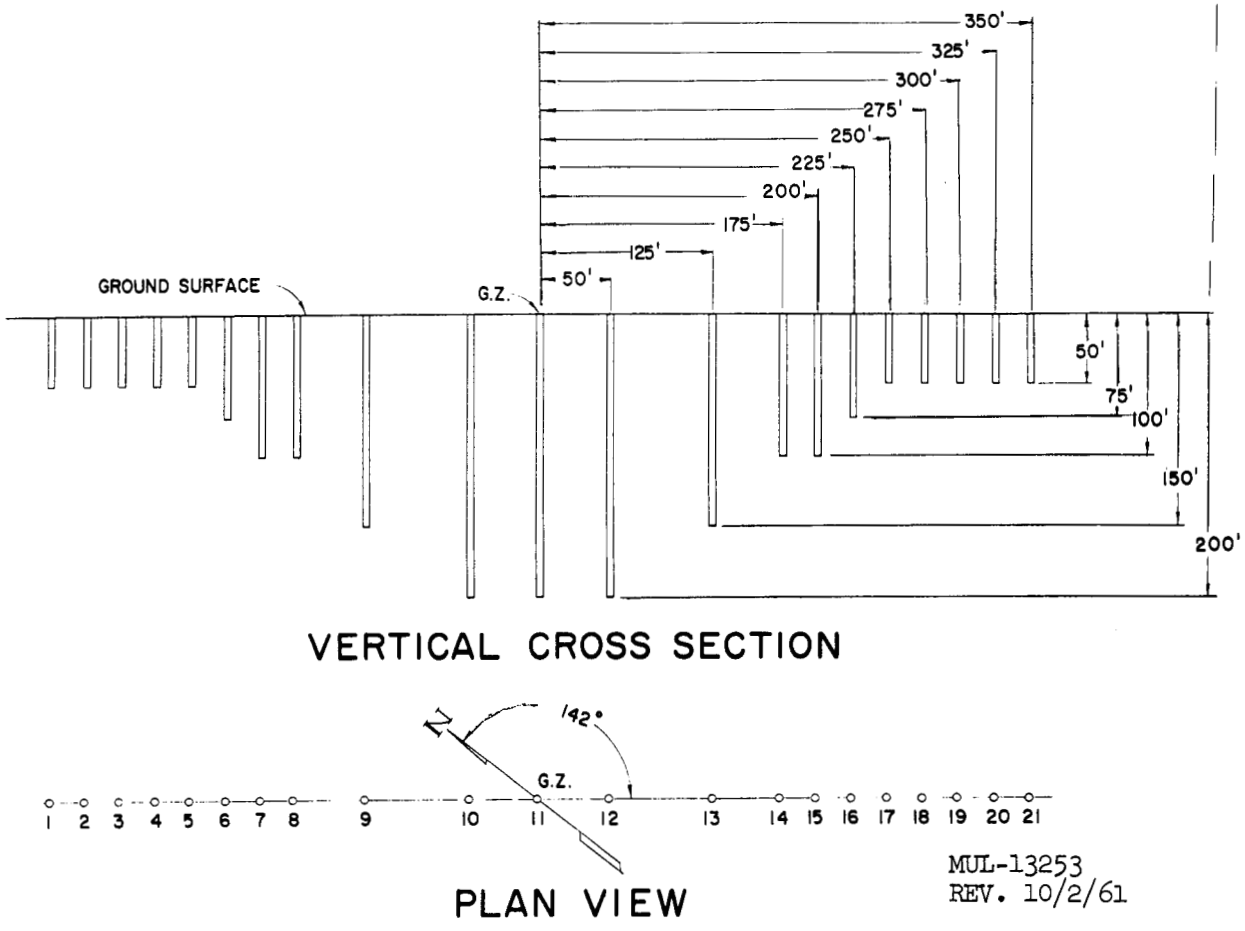

Fig. 3. Preshot locations of sand columns for Teapot ESS.

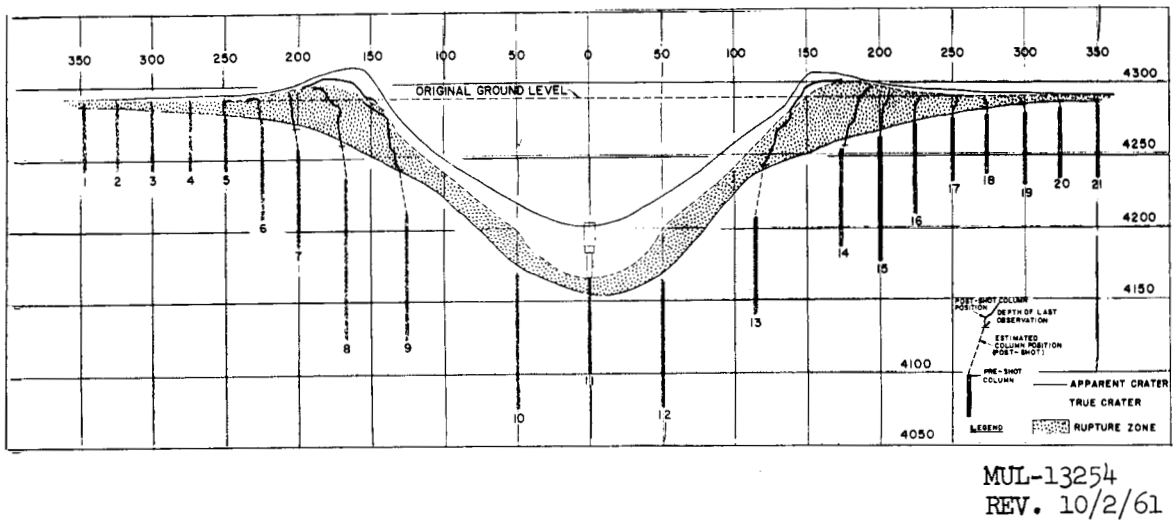

Fig. 4. Postshot locations of sand columns for Teapot ESS.

Fig. 5. Aerial view of Area 10 showing craters.

of columns 9 and 13, which were extended and folded back over the edge of the true crater. The other columns show very strong effects of shear and rupture. From these data, the depth of the true crater is believed to be 128 feet and the radius 150 feet. The depth of the rupture zone can only be estimated, but its radius is believed to be 250-275 feet.

Figure 5 is an aerial view of Area 10 showing Teapot ESS and Jangle U in top center. The trench in Teapot ESS is clearly visible. The recent high-explosive alluvium craters described below, including Scooter in the lower center and the three Stagecoach craters on the left, are also visible.

Neptune. The Neptune event occurred during Operation Hardtack, Phase II, on 14 October, 1958.[19] It was a 115-ton nuclear device fired at a point 100 feet below a 30° slope in bedded tuff. The vertical distance to the surface was 110 feet. The zero point room was 12 × 17 × 10 feet high with a concrete floor. The tunnel was shaped like a buttonhook and was stemmed before the shot in several places with sandbag plugs.

Upon detonation, the surface rose in a hemispherical dome to a height of 25-35 feet, at which time it was disrupted by ejected material and venting gas, with large rocks going 80-100 feet in the air. A large dust plume was formed, which rose to a height of about 1000 feet. A large mass of rock and debris cascaded down the slope, carrying small amounts of radioactivity into gullies to distances downhill (upwind) on the order of 2000 feet.

The shape of the crater formed by the Neptune detonation was influenced by the slope of the surface in that almost all of the debris formed a slide originating at the lower edge of the crater and terminating about 800 feet down the slope. The mean diameter was 200 feet and the maximum depth was 35 feet.

A total of 11 holes have been drilled into the region surrounding the Neptune detonation to determine the physical state of the rock and to delineate the radioactive regions.[20] Figures 6 and 7 show these holes and the picture of the postshot state of the medium derived from them. Most of the layers overlying the shot have retained their continuity but have collapsed into the cavity produced by the explosion. The mixing that occurred was minor and the different lithologic units are still easily identifiable.

Crushing of the tuff occurred to a distance of 40 feet downward and 50 feet laterally except in the direction of the original drift, where crushing

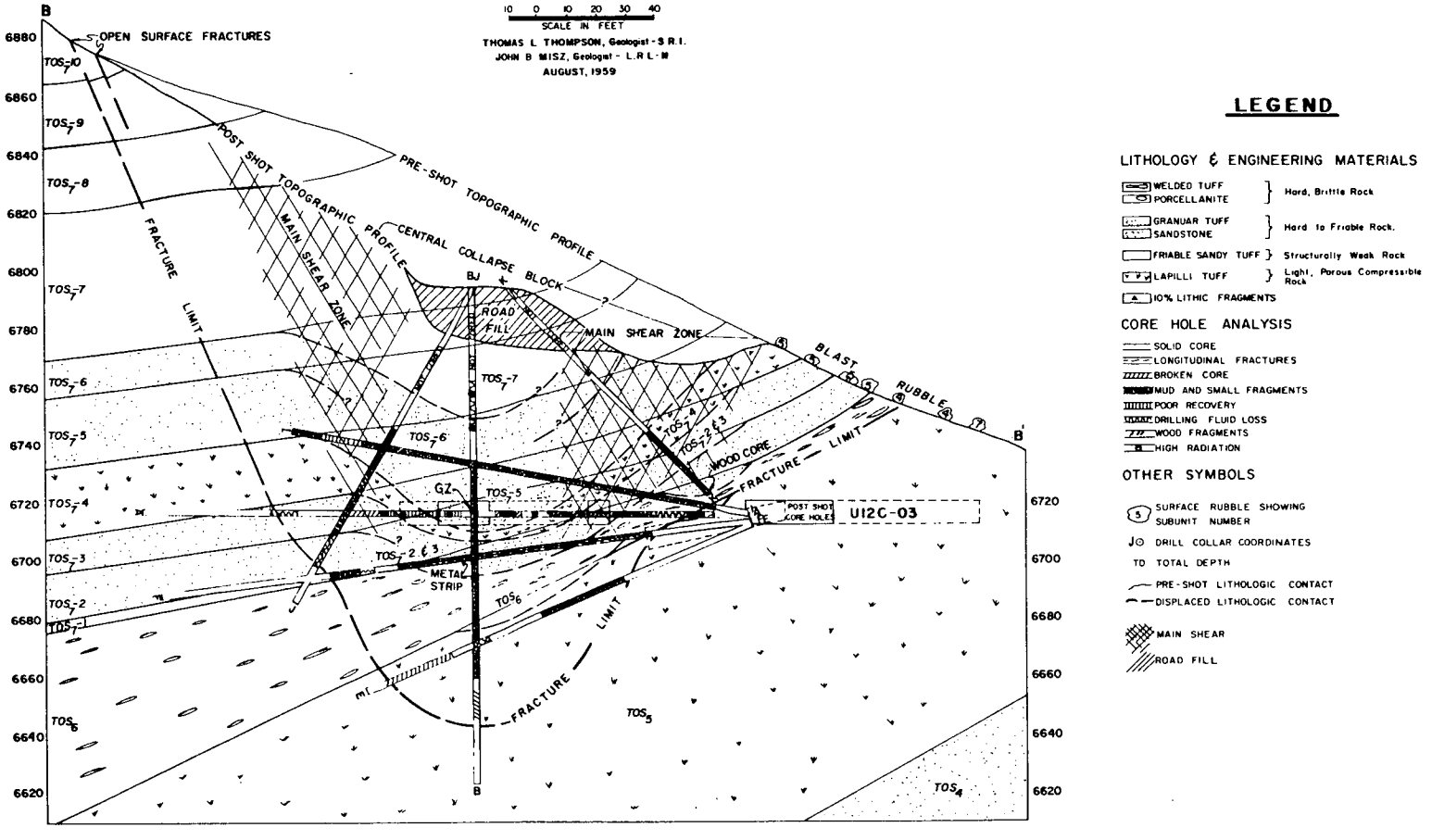

MUL-9189

Fig. 6. Neptune cross section B-B'.

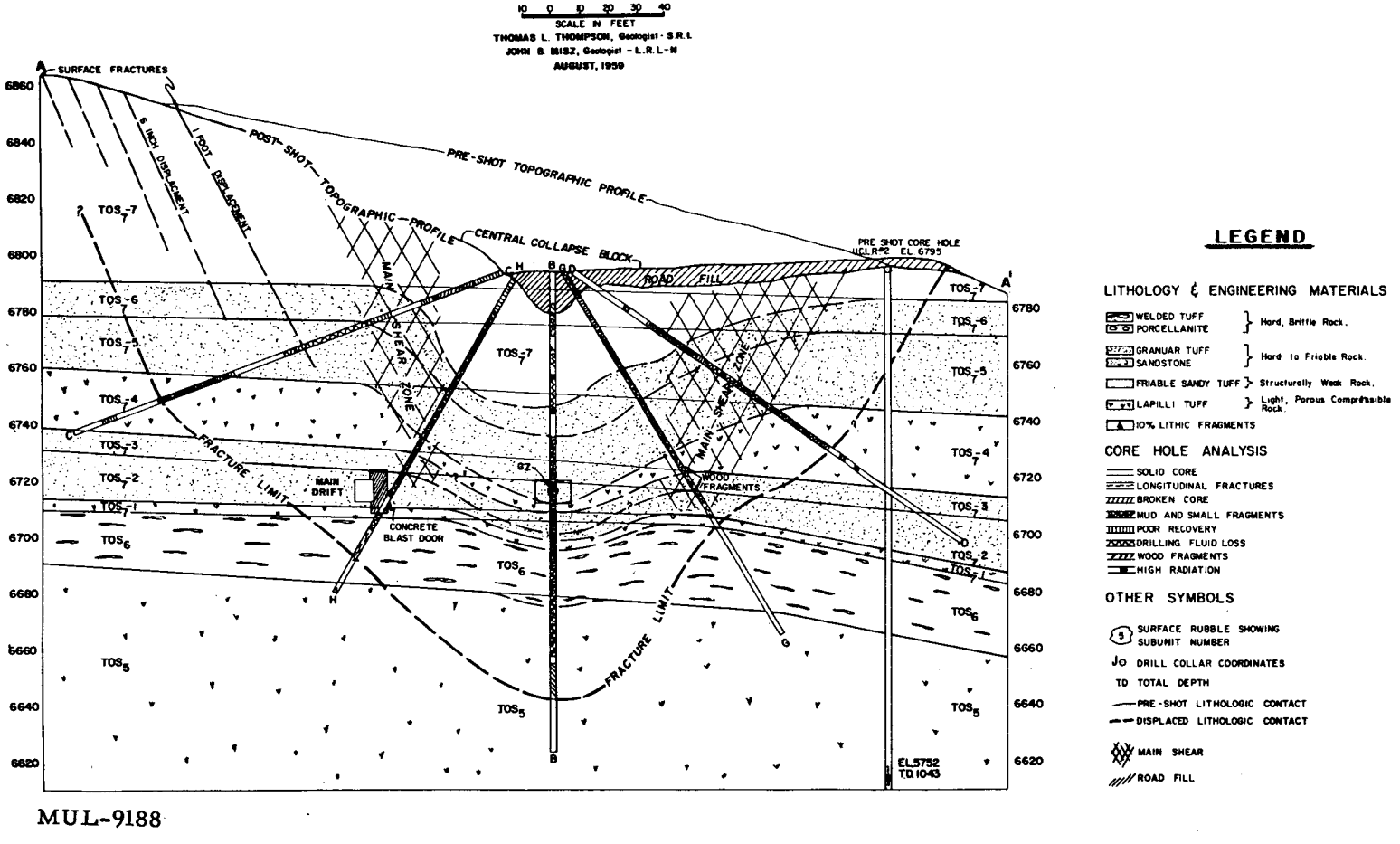

MUL-9188

Fig. 7. Neptune cross section A-A'.

extended to 80 feet. The extent of crushing was apparently influenced by bedding plane weaknesses. Fracturing of the material extended to 70 feet in the hemisphere below the zero point, according to current interpretations of core data. Above the original zero point, fracturing extended to the surface, with the boundary of fracturing lying on a cone whose top extended slightly beyond the surface crater region.

Integration of the total fallout patterns on the surface indicated that 1/2% of the total fission product activity produced by the explosion escaped from the crater.* Due to the presence of certain volatile isotopes at early times, this activity is enriched by a factor of 5 in Sr^{90}, and Cs^{137}.

Radioactivity Release

On the basis of the above four nuclear cratering explosions, and the deeply buried Blanca detonation[21] which released 0.05% of its activity to the atmosphere,* a curve showing the fate of activity released as a function of the ratio of depth of burst to crater depth has been drawn (Fig. 8).[22] This abscissa has been chosen to make the data applicable to a wide range of media. As can be seen from Fig. 8, for those depths of burst where the crater depth is half the depth of burial of the charge, the fraction of radioactivity that is released to the atmosphere and appears as prompt fallout is only 3 to 4% of the total activity produced. This fraction will be enriched in certain isotopes with volatile precursors, such as Sr^{90}, by a factor of about 5. When thermonuclear explosives are used, in which only 5% of the yield comes from fission, the above fraction applies only to this fission contribution, and hence the total activity release corresponds to an extremely small fraction of the total yield (0.15-0.20%). Activity induced in the medium surrounding a thermonuclear explosion by the high energy neutrons that are released can be reduced below this value by standard neutron shielding procedures.

Air Blast

Measurements made in the Stagecoach, Buckboard, and Scooter high explosive detonations show that close-in air blast was attenuated by a factor

*This fraction of percentage release differs from earlier published values because of recent renormalization of the definition of activity produced per kiloton of fission yield (see ref. 22).

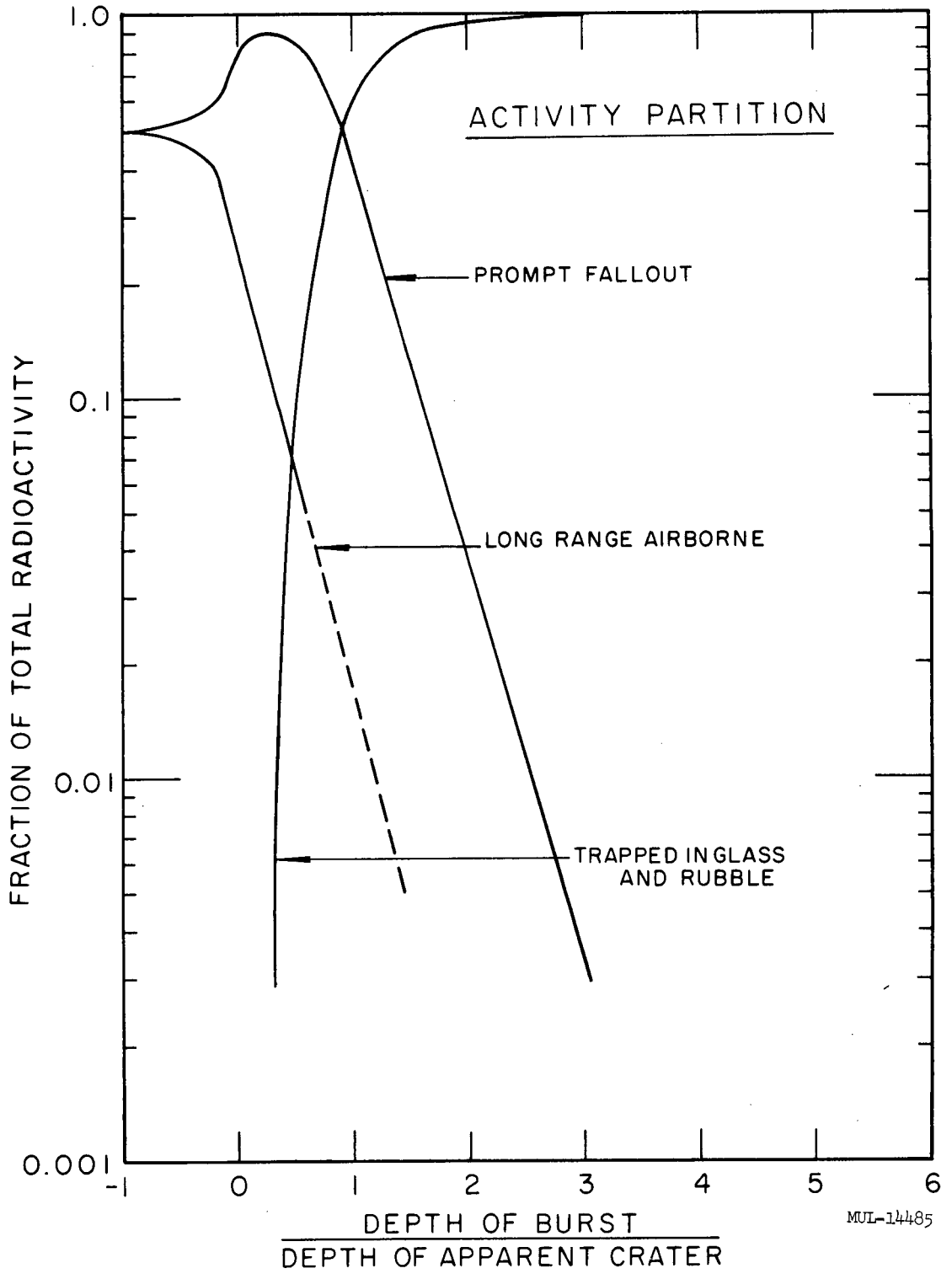

Fig. 8. Radioactivity release as a function of ratio of depth of burst to depth of apparent crater.

of over 100 for an explosive placed at or below optimum depth of burst, (i.e. that depth at which maximum crater dimensions are produced). Similar measurements on long range air blast, which is produced by tropospheric or ozonospheric reflection of sound waves back down to the earth at ranges of 50-150 miles, shows that it is attenuated by a factor of 5-10 by burial at or below optimum depth.

CHAPTER III. HIGH EXPLOSIVE CRATERING EXPERIENCE

Brief Summary of Early H.E. Experience

Perhaps the first cratering experiments with large size H.E. charges were conducted by the British in the early 1940's using TNT bombs. Much work was also done in this country in 1943-1945 by the National Defense Research Committee at Princeton[23] in which, for the first time, underground measurements were made of pressures, accelerations, and displacements in a variety of media. Charge sizes ranged from 8 to 3200 lb.

The Panama Canal Company initiated a series of high-explosive cratering programs in 1947 to determine the vulnerability of the Panama Canal to attack by nuclear weapons. These programs, each of which included 15 to 20 shots, were performed in basalt,[24] sandstone,[25] clay,[26] water-saturated marine muck,[27] and an alluvial sand-gravel mix termed cucaracha and culebra.[28] Measurements were made of all pertinent parameters, including apparent and true crater dimensions, extent of the rupture, permanent displacement and elastic zones, and distance of debris ejection. Unfortunately, only cylindrical charges ranging from 8 to 200 lb were used and thus the scatter of the data for the rock media was very large ($\pm$ 25% for radii and $\pm$ 50% for depths).

Starting in 1948 and continuing somewhat intermittently until 1951 was the Underground Effects Tests Program, (UET), which was sponsored by the Corps of Engineers and conducted largely at the Dugway Proving Grounds in Utah. The UET program was fielded by several agencies, including Stanford Research Institute (SRI) and Engineering Research Associates (ERA). Charges ranging from 8 lb to 320,000 lb of TNT were used, generally made up by stacking blocks in the shape of a sphere. Many materials were studied, including soil, granite, sandstone, and limestone. A large number of underground free-field measurements were also included in these programs.

In 1951, the first of a long series of high-explosive cratering programs in alluvium was performed as part of the Buster-Jangle nuclear test series. These programs in alluvium, extending in time from 1951 to 1960, will be outlined in more detail below.

The results of the above programs, as well as those of many small-scale programs which I have omitted, are given in an excellent summary of cratering data published by the U. S. Army Engineers Waterways Experiment

Station.[29] Unfortunately many of the above data were taken under conditions that make them difficult to use here. In some cases only true crater dimensions were measured. In others, cylindrical charges or very small charge weights were used, which make the data unreliable for extrapolation to large nuclear yields. For these reasons the rest of this report will concentrate on the voluminous data taken in NTS desert alluvium, with only minor references to results in other media.

Desert Alluvium H.E. Cratering Experience

In conjunction with the Jangle and Teapot cratering explosions, several high-explosive cratering programs were conducted in 1951 in the desert alluvium of Area 10 at NTS, the site of the above nuclear craters.[30] Charges ranging from 256 lb to 40,000 lb of TNT were used. The first of these programs, designated as the Jangle H.E. series, was executed in 1951 and consisted of nine 2560-lb shots and one 40,000-lb shot, all at shallow depths of burst to simulate the Jangle U and Jangle S nuclear shots. The charge configurations were approximately spherical, being built out of 100-lb blocks of TNT. A summary of the experimental data from this series as well as from the rest of the high-explosive cratering programs in desert alluvium can be found in Appendix A. In addition, all of the data from desert alluvium have been plotted in Figs. 9 and 10 using $W^{1/3}$ scaling to correlate the data from shots using differing charge weights.

In 1952, additional cratering results as well as data on other effects were obtained by a cratering program in NTS desert alluvium named the Mole Series,[31] conducted by Stanford Research Institute for the U. S. Army Corps of Engineers. For this series seven 256-lb spheres of cast TNT were used, with depths of burial ranging from slightly above the surface to 6.35 feet below the surface. This series was the first program to give significant cratering data for moderately well-buried charges in desert alluvium. At approximately the same time as the above series in desert alluvium was being conducted, another phase of the Mole program involving a similar series in moist and dry clay was being performed. However, it was confined to shallow depths of burst.

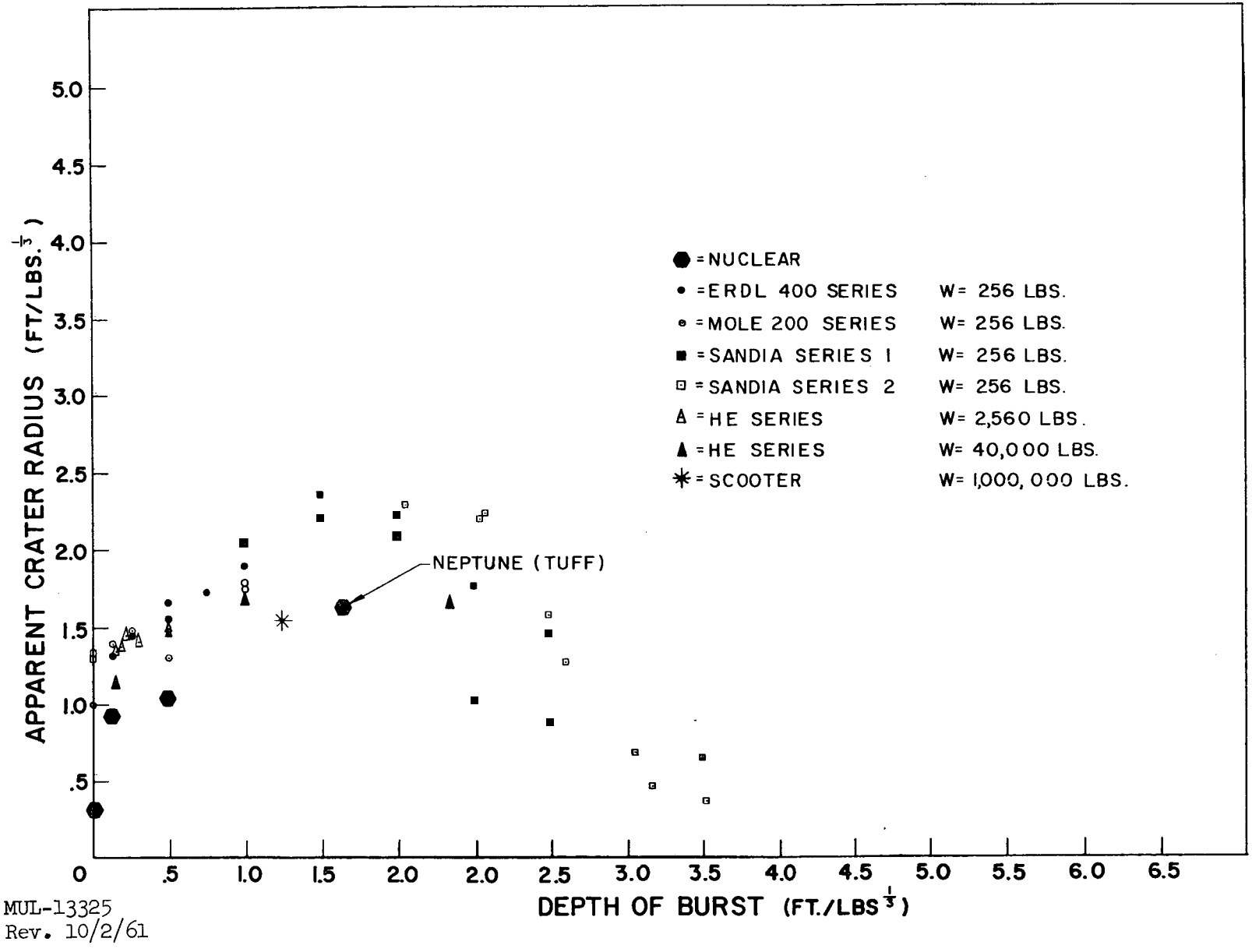

Fig. 9 Apparent crater radius vs depth of burst for NTS alluvium, $W^{1/3}$ scaling.

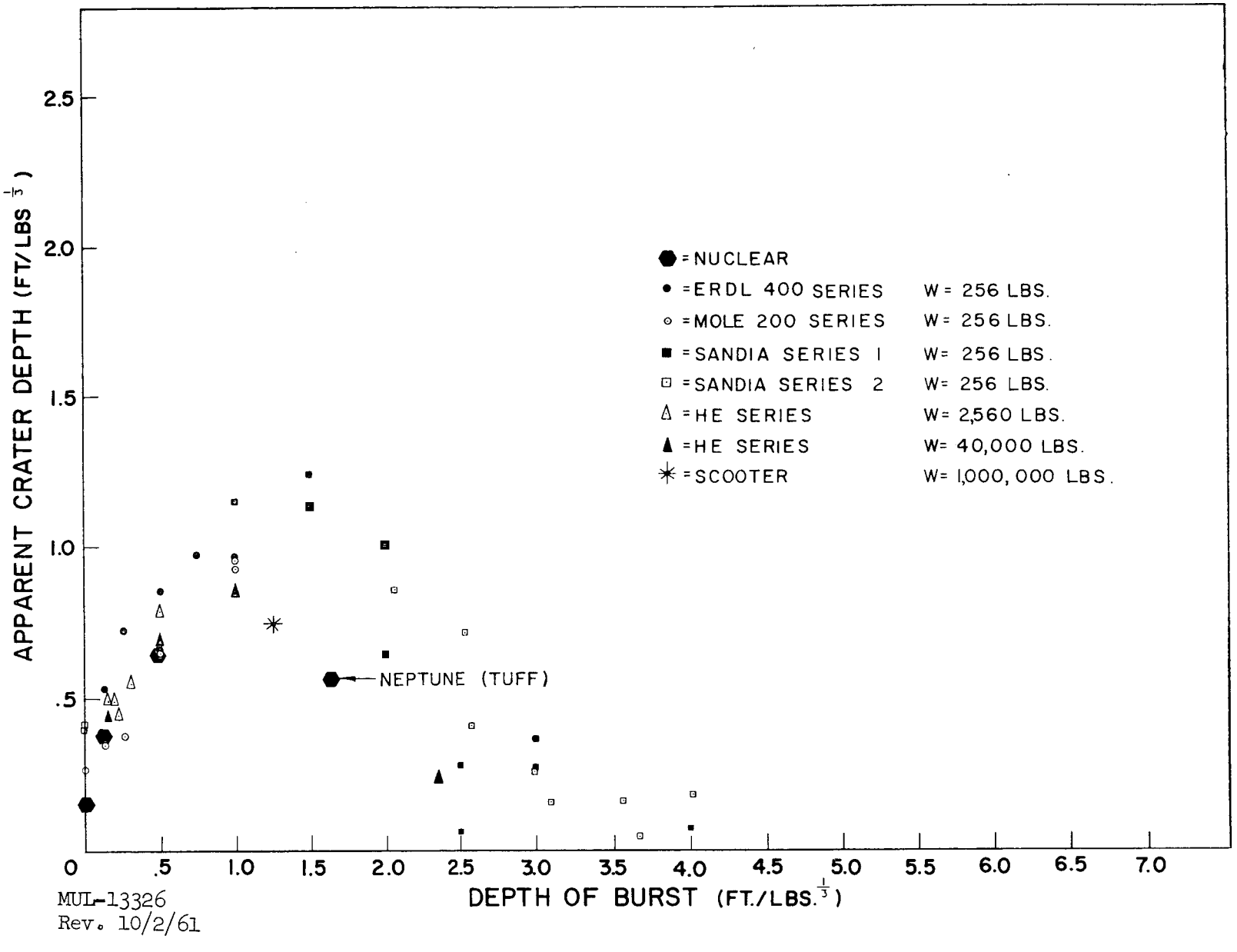

Fig. 10. Apparent crater depth vs depth of burst for NTS alluvium, $W^{1/3}$ scaling.

To obtain more data in the region of scaled depth of burst of the proposed Teapot ESS nuclear cratering explosion, Engineering Research and Development Laboratories (ERDL) executed a program[18] in the fall of 1954 which was very similar to the above Mole program in desert alluvium. For this program, the ERDL 400 series, six 256-lb cast TNT spheres were used at depths ranging from 0.83 to 6.35 feet, with two at the scaled depth of the nuclear shot. Considerable effort was devoted to investigating true crater dimensions for this program in anticipation of the major program of true crater delineation planned for the nuclear shots.

Thus are summarized the data available when the Plowshare Program was instituted in 1958.[32] These existing data were only of limited usefulness in designing Plowshare experiments, however, because they were obtained with too shallow depths of burst. As can be seen from Figs. 9 and 10, no shots had been fired at a deep enough depth of burst to locate the peak of the radius or depth curves. To obtain such data, a cratering program was performed by Sandia Corporation in the spring of 1959 which included ten 256-lb cast TNT spheres buried at depths ranging from 6.35 feet to 25.4 feet.[33] Because of increased scatter of the data at the larger depths of burst, this program was followed in the fall of 1959 by a second phase that essentially repeated the work of the first phase but improved the statistics.

Stagecoach. In the spring of 1960, the Stagecoach program[34] was initiated to better define the correct scaling laws at scaled depths of burst that spanned the depth of burst curve. The program, sponsored by the AEC and fielded by Sandia Corporation, was composed of three detonations, each with a charge weight of 40,000 lb of TNT. The charges were made up of 36-lb blocks of TNT stacked to form a sphere. The depths of burst measured to the centers of the spheres, were 17.1, 34.2, and 80 feet. The preliminary results of the detonations are given in Table II, and are shown in Figs. 9 and 10 by the triangular points at scaled depths of burst of 0.5, 1.0, and 2.3 ft $(lb)^{1/3}$. Cross sections of these three craters are shown in Fig. 11.

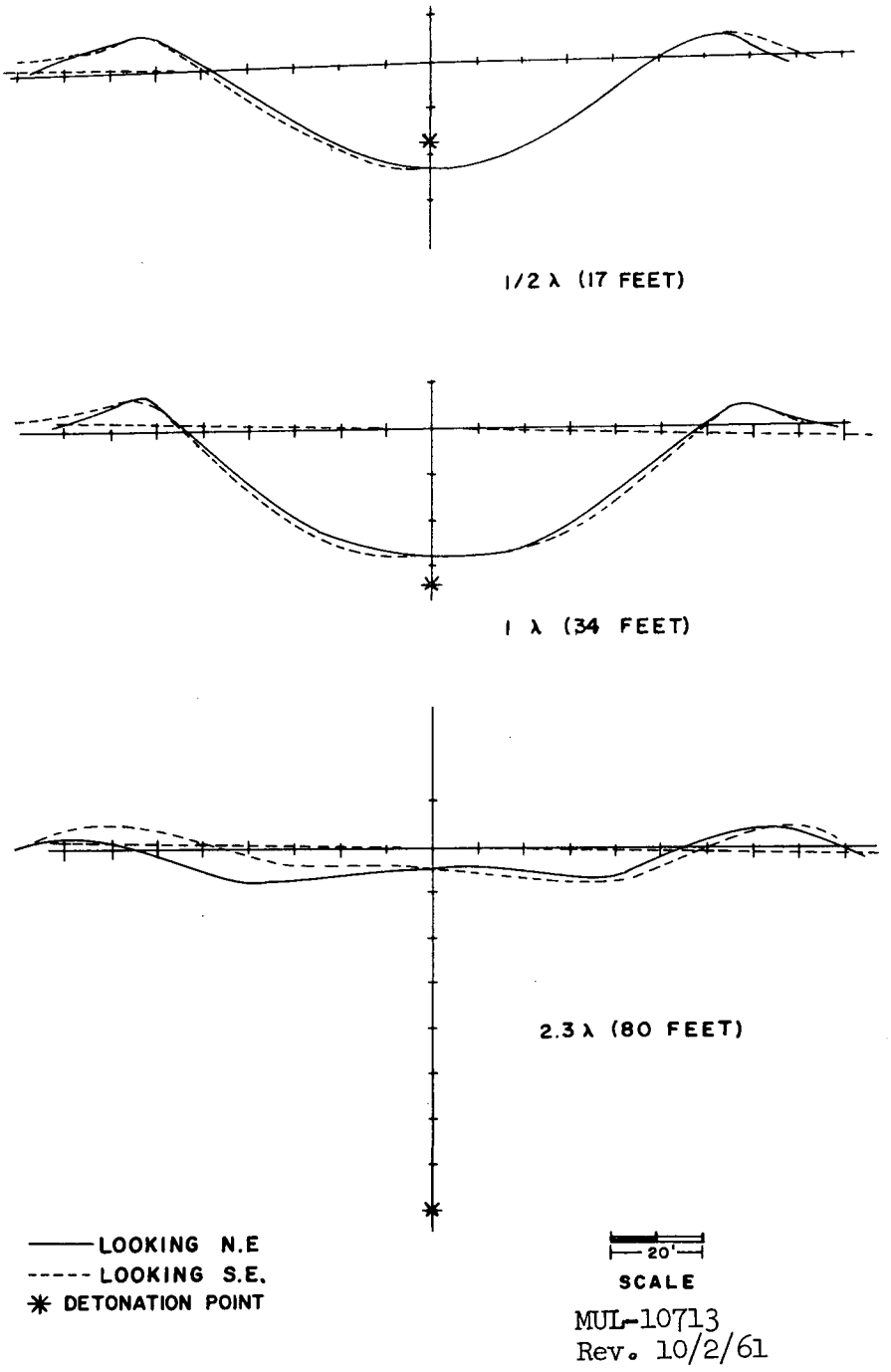

Fig. 11. Stagecoach crater profiles.

Table II. Results of Stagecoach cratering program with 40,000-lb TNT charges in desert alluvium at Nevada Test Site (see ref. 35).

Shot No.	Depth Burst (ft)	Apparent Crater Radius (ft)	Apparent Crater Depth (ft)	Apparent Crater Volume (yd^3)
2	17.1	50.5	23.6	3100
3	34.2	58.6	28.2	5360
1	80	57.0	7.0	1820

Several interesting observations can be made regarding the shapes of these craters. Stagecoach shot No. 2 (20-ton yield) had the same scaled depth of burst as the 1200-ton Teapot ESS nuclear shot (0.5 ft $(lb)^{1/3}$), but it produced a crater whose scaled radius was much larger than Teapot ESS's (see Figs. 9 and 10), while the scaled depths of the two craters were about equal. This would indicate that as one goes to larger yields at the same scaled depth of burst, the ratio of radius to depth decreases. The same trend, although not as obvious as in this example, can be seen in earlier data.

The deep crater, from the shot at 80 feet, also shows some interesting characteristics. As can be seen from the shape of the crater shown at the bottom of Fig. 11 and from the high speed photographs of the detonation, this crater resulted, to a very great degree, from plastic deformation and rupture of the alluvium surrounding the detonation point, followed by subsidence of the overlying material into the crater when venting of the gas ball occurred. The resulting crater is very shallow and flat-bottomed, but very wide. However, when this crater is scaled to a 100-kiloton charge, the radius and depth are adequate for many Plowshare applications such as harbors and canals. The mechanism of cratering at this scaled depth of burst is well suited to retain a very large fraction of the radioactivity produced in a nuclear detonation.

Scooter. Inspection of the data shown in Figs. 9 and 10 reveals that, while there is a large scatter of the data, there is a consistent trend for the large-yield, high-explosive data to fall below the 256-lb data. In an attempt to better correlate the high explosive data, Vaile in 1955 proposed the use of $W^{1.3.4}$ instead of $W^{1/3}$ as a scaling factor.[15] His work was based on the single 2560-lb shot at the Teapot scaled depth and the 2560- and 40,000-lb shots at the Jangle U scaled depth. As will be shown later in this report,

the Stagecoach data lead to essentially the same result.

The design of nuclear excavation projects envisages the use of nuclear explosives with yields of 10 kilotons or greater. Since the larger yields require larger depth of burst, the effects of gravity become more important, although to an uncalculable degree. In addition, the effects of strength of materials and internal frictional forces become less important. To ensure that the use of $W^{1/3.4}$ scaling of the lower yield data to these yields and larger would not be seriously in error, the Scooter project was proposed.

This experiment, which was sponsored by the Lawrence Radiation Laboratory as a part of the Plowshare Program and fielded by Sandia Corporation, consisted of 500 tons of TNT buried at a depth of 125 feet in the desert alluvium of Area 10 at NTS, close to the Jangle U and Teapot ESS craters. The charge consisted of blocks of TNT stacked to form a sphere. A detonator was placed at the center of the sphere, 125 feet deep.

Scooter was detonated at 0715 PST on October 13, 1960. The resulting apparent crater had an average radius of 153.8 feet and a depth of 74.5 feet.[35] The total volume of the apparent crater was about 100,000 cubic yards. These results agree to within a few percent of the prediction made before the shot, based on $W^{1/3.4}$ scaling. Thus, the preliminary results indicate that $W^{1/3.4}$ scaling is adequate to predict crater dimensions in the kiloton range of yield, and that no serious error will result in extrapolating this law into the 10-kiloton range.

Accompanying the Scooter detonation were many additional experimental programs such as air blast, ground surface motion, seismic measurements, particle trajectory, and throwout distribution studies. The results of these programs are not yet complete but they will significantly increase our knowledge of these phenomena.

Results From Other Media

Proper design of nuclear excavation projects requires a knowledge of the cratering characteristics of a wide variety of media. There have been numerous cratering programs in the past in media ranging from saturated marine muck to basalt. Unfortunately, as outlined above, many of these data are not applicable either because of failure to measure apparent crater dimensions, concentration of data at shallow depths of burst, unusual charge shapes, or the use of too small charge weights. The only programs whose

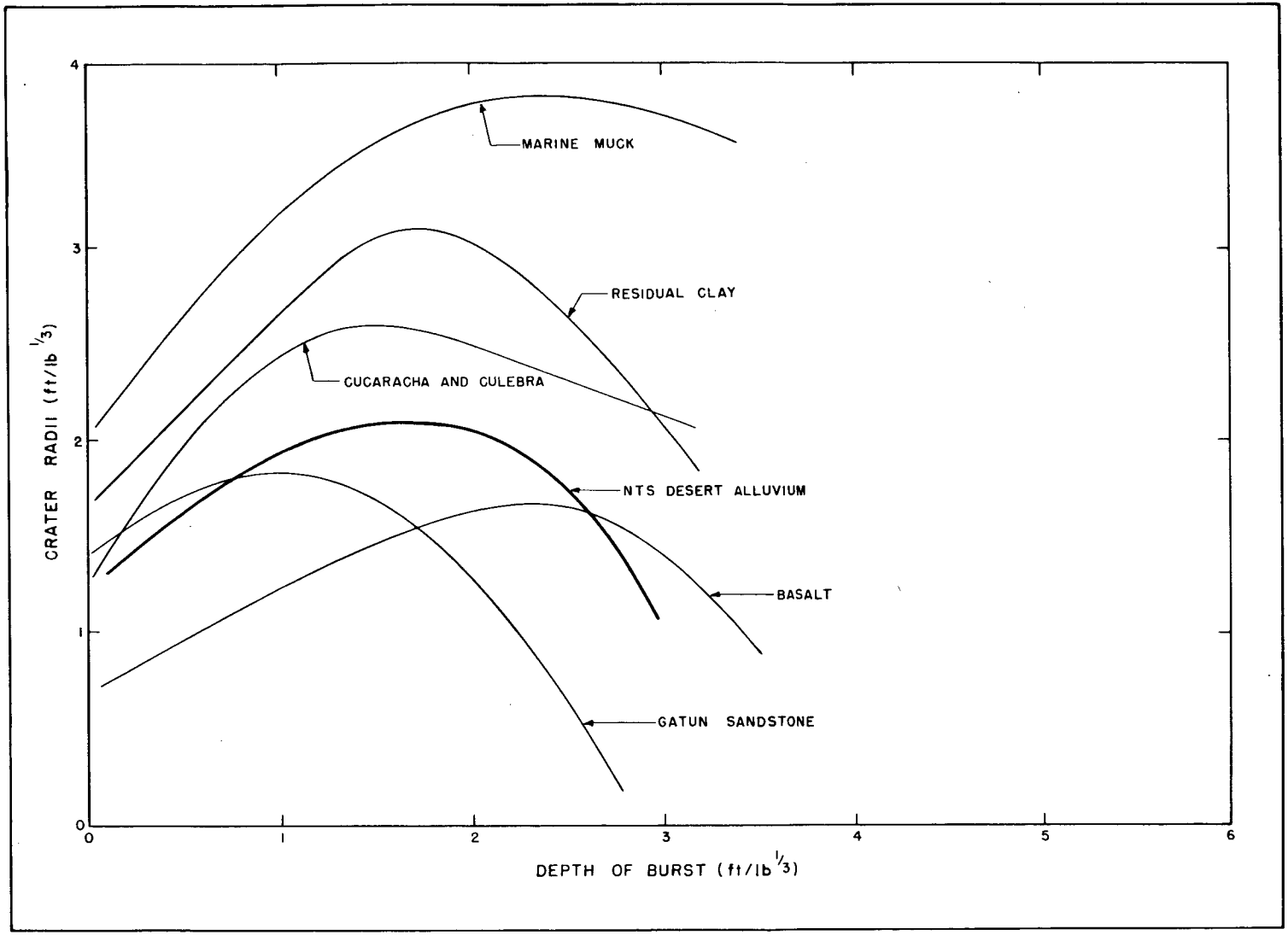

MUL-10651
Rev. 10/2/61

Fig. 12. Crater radius vs depth of burst for six materials, including Isthmian Canal Studies data ($W^{1/3}$ scaling).

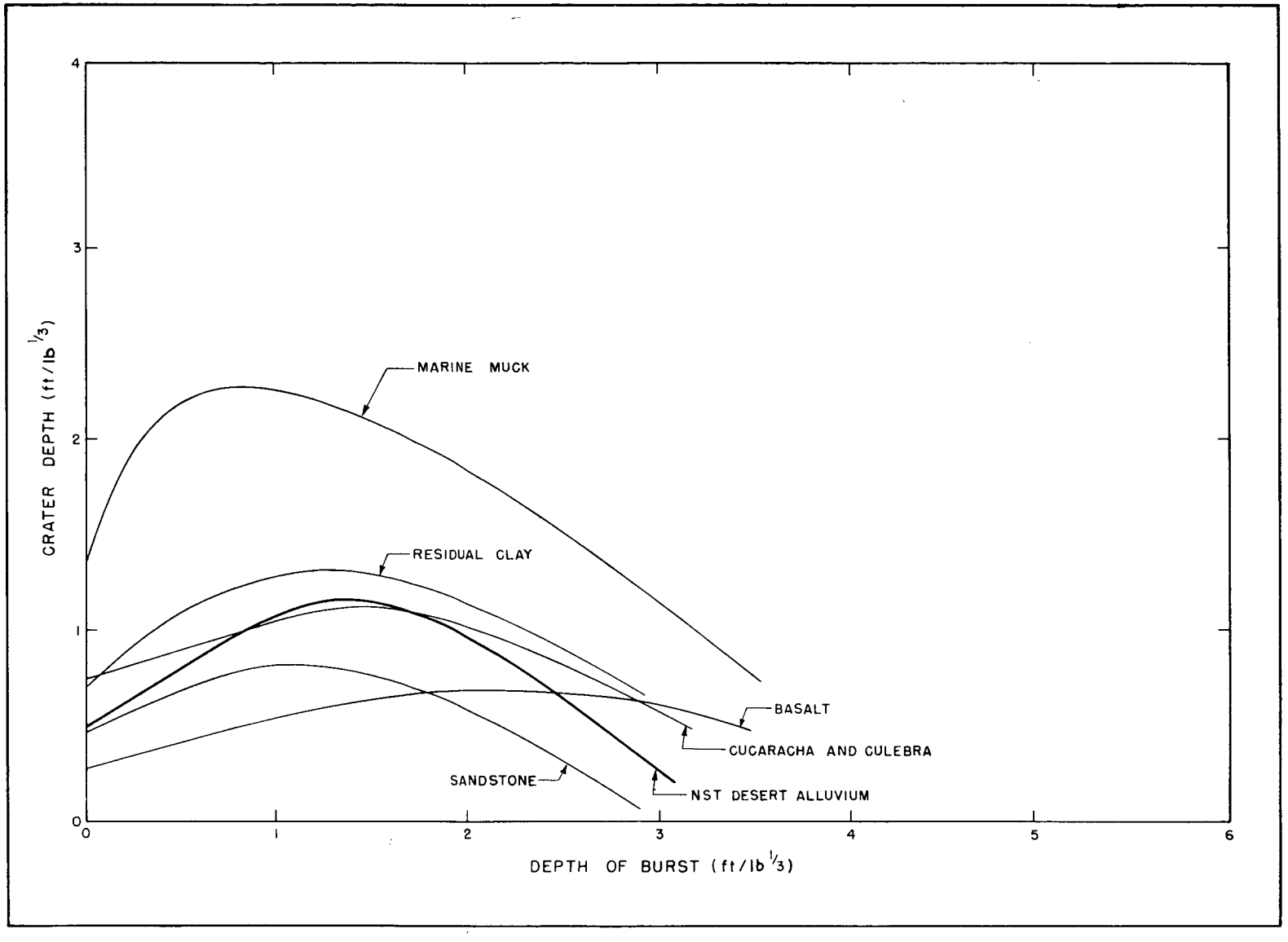

MUL-10650
Rev. 10/2/61

Fig. 13. Crater depth vs depth of burst for six materials, including Isthmian Canal Studies data ($W^{1/3}$ scaling).

results are at all useful to Plowshare are the cratering studies conducted by the Panama Canal Company; these results are summarized in Figs. 12 and 13, where least-squares fits to the data have been plotted. Here, because of the small range of the yields involved, the data are plotted as a function of scaled depth of burst using $W^{1/3}$ scaling. For comparison purposes an approximate fit to the NTS desert alluvium data has also been plotted here as the heavy dark line.

Buckboard

To obtain cratering data for hard rock that would be useful to the Plowshare Program, the Buckboard project[11] was undertaken in the summer of 1960. Sponsored by Plowshare and executed in the field by Sandia Corporation, it consisted of 10 1000-lb and 3 40,000-lb detonations in basalt. The site was the basalt-topped 40-Mile Canyon mesa at NTS. Scaled depths of burst for the 1000-lb shots varied from 0.5 ft $(lb)^{1/3}$ to 2.5 ft $(lb)^{1/3}$, with two shots at each depth. The three 40,000-lb shots were at scaled depths of burst of 0.75, 1.25, and 1.75 ft $(lb)^{1/3}$.

The preliminary results of this program are plotted in Figs. 14 and 15. As can be seen, the maximum crater radius is about the same as for the I.C.S. basalt data in Fig. 12 i.e., 1.5 ft/$(lb)^{1/3}$. The location of the maximum of the depth of burst-vs-radius curve appears to be at a much shallower depth of burst. However, it should be mentioned that for the deep 1000-lb shots on Buckboard, the cement stemming failed, and pieces of stemming were observed going over 500 feet in the air. This undoubtedly had an effect on the crater dimensions of the deeper craters, but its effect is very difficult to evaluate. This difficulty was corrected for the three 40,000-lb detonations. The scatter of the data for the 1000-lb shots would appear to be about ± 25%, and it is very difficult to draw a meaningful curve through these data.

The depths shown in Fig. 15 are about the same as the I.C.S. data but the scatter is obviously very bad, pointing to the conclusion that 1000-lb or smaller charges are unsatisfactory for cratering programs in hard rock media. The scatter of the data is due to the large block sizes of the fallback and the resulting porosity, which makes necessary a prohibitively large number of craters to obtain statistically accurate results with small charges.

The three 40,000-lb detonations resulted in craters whose dimensions are given in Table III. These dimensions are many times larger than the

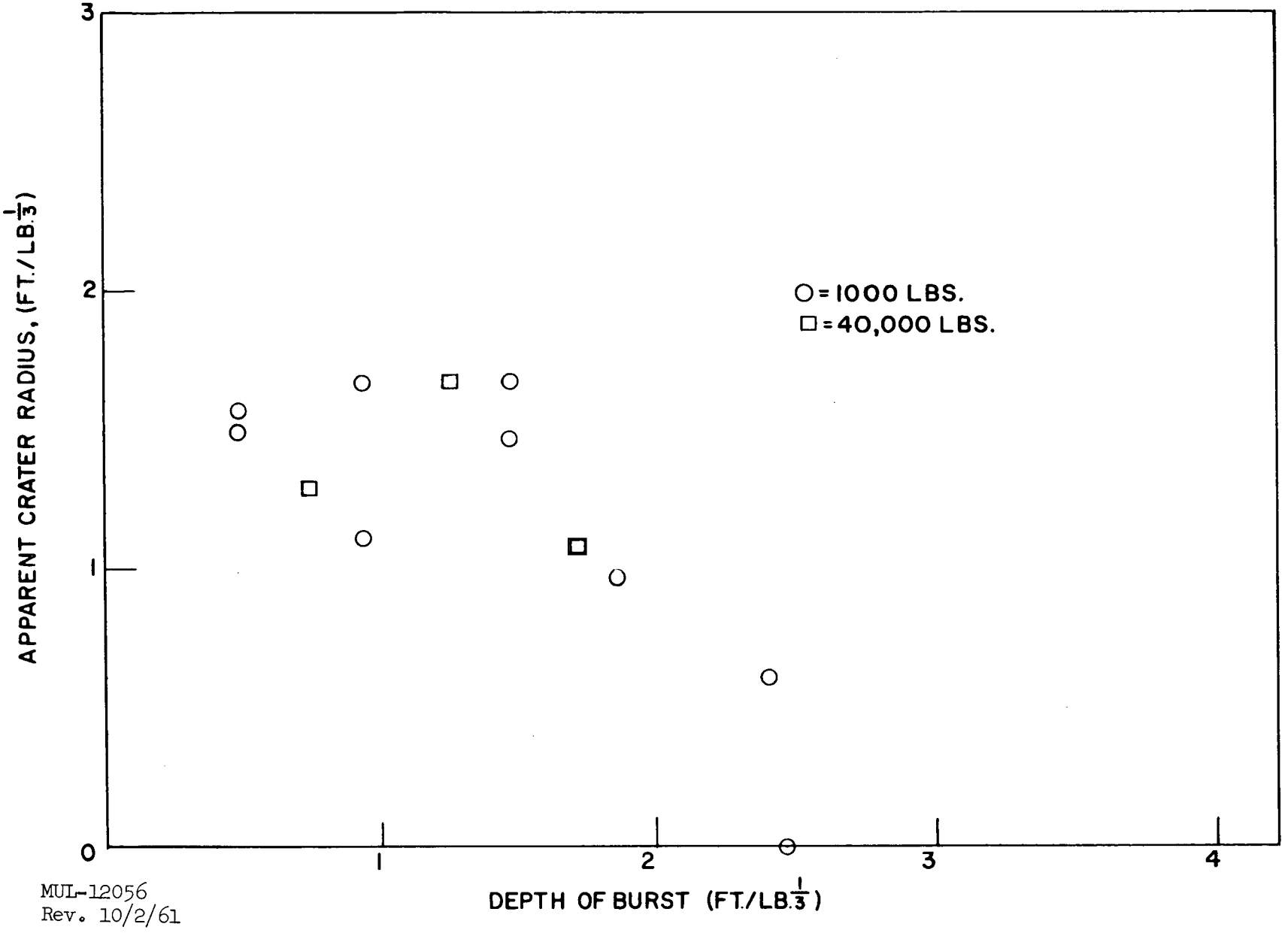

Fig. 14. Crater radius vs depth of burst for basalt, from Buckboard ($W^{1/3}$ scaling).

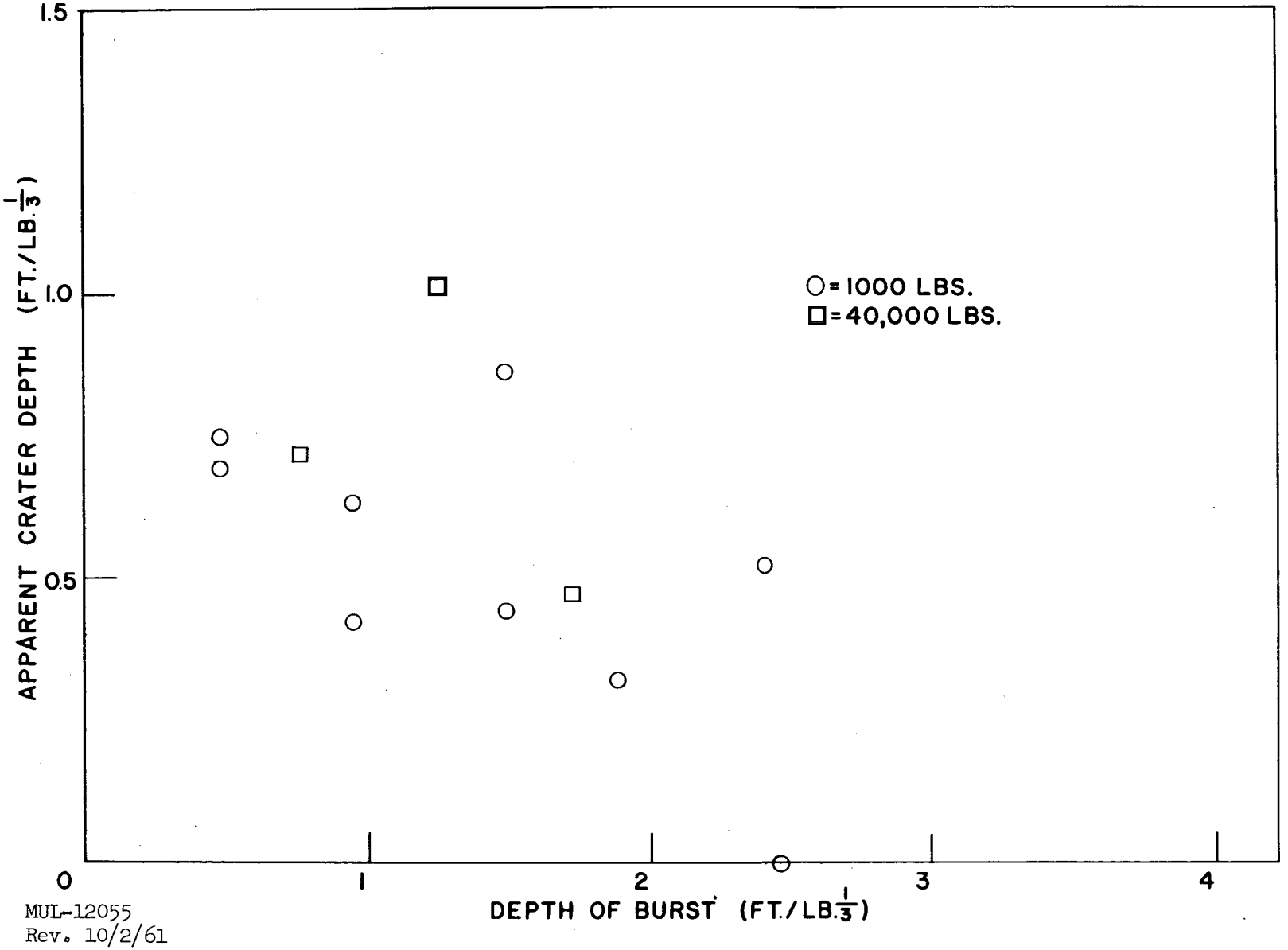

Fig. 15. Crater depth vs depth of burst for basalt, from Buckboard ($W^{1/3}$ scaling).

average block size of the debris, and hence these craters are better models of large-scale nuclear craters.

Table III. Results of Buckboard cratering program with 40,000-lb TNT charges in basalt at Nevada Test Site (see ref. 35).

Shot No.	Depth of Burst (ft)	Apparent Crater Radius (ft)	Apparent Crater Depth (ft)	Apparent Crater Volume (yd^3)
11	25.5	44.6	24.9	2370
12	42.7	57.0	34.7	5000
13	58.8	36.8	16.2	860

The large scatter of the 1000-lb craters also makes determination of any deviation of the scaling law from $W^{1/3}$ for basalt impossible. However, there is no reason to believe that a scaling law derived from alluvium would be incorrect for basalt.

As with the earlier Scooter detonation, there were several programs such as air blast, throwout, and particle trajectory studies accompanying the three 40,000-lb programs. Results of these programs will aid greatly in predicting these phenomena in hard rock media.

CHAPTER IV. ANALYSIS OF DESERT ALLUVIUM DATA

The large amount of cratering data available for the single medium, NTS desert alluvium (see Figs. 9 and 10), allows a quite complete analysis to be made of its cratering characteristics. The approach in this analysis has been to assume that an empirical scaling law can be found that will satisfactorily correlate the data from craters obtained with different size charges of high explosives (TNT). It is further assumed that nuclear and high-explosive craters would then obey similar scaling laws. By comparison, it is then possible to calculate a nuclear-high explosive efficiency (i.e., the ratio of the high explosive yield to nuclear yield required for an equivalence of cratering effects). Since there are two independent data points from any one crater, the radius and the depth, two values for an empirical scaling exponent or efficiency are obtained. The significance of this point will be discussed at the end of this section.

Symbols and Terms

At the present time there exists no universally accepted system of units or symbols for discussing cratering. For the purposes of this paper I have defined a set of symbols which are consistent with most common usage and appear to be of greatest utility. The actual dimensions of the apparent crater are defined as:

R = apparent crater radius (ft),

D = apparent crater depth (ft),

and

Z = actual depth of burst of charge (ft).

Negative values for Z indicate distances above the ground surface to the center of gravity of the charge.

Two terms that are universally used when discussing cube-root scaling of cratering data are λ and λ_c:

λ = any dimension related to a crater when scaled by cube-root scaling = $\text{dimension} / \left[W^{1/3} \text{ ft (lb)}^{1/3} \right]$. In general usage, a crater dimension or the distance from the charge may be referred to as being "$n\lambda$", meaning a distance equal to $n \times \left(W^{1/3} \text{ ft} \right]$, where W is the charge weight in pounds of TNT.

λ_c = scaled depth of burst expressed in terms of λ, being equal to $Z \; W^{1/3} \left[\text{ft (lb)}^{1/3} \right]$.

To eliminate confusion over the type of scaling being used to present data, it has been found necessary to adopt a standardized procedure. Thus, when using cube-root scaling, charge weights are expressed in pounds of TNT and crater dimensions are then expressed in terms of λ. When using empirical scaling as derived here and elsewhere, charge weights are expressed in kilotons of TNT. The basis for this convention is that when one is comparing the results of experimental program using charges ranging from 1 to 10^3 lb, cube-root scaling is adequate, whereas when charge ranges of 10^6 - 10^8 lb (0.5-50 kt) are being discussed, an empirical scaling law has been found necessary. Using these conventions, we have for cube-root scaling:

$\lambda_c = z_s$ = scaled depth of burst, cube-root scaling, $ft/(lb)^{1/3}$,

r_s = scaled apparent crater radius, cube-root scaling, $ft/(lb)^{1/3}$,

d_s = scaled apparent crater depth, cube-root scaling, $ft/(lb)^{1/3}$.

For treatment of the data by empirical scaling we have:

$Z_s = Z/W^{1/p}$ = scaled depth of burst, pth root scaling, $ft/(kt)^{1/p}$,

$R_s = R/W^{1/p}$ = scaled apparent crater radius, pth root scaling, $ft/(kt)^{1/p}$,

$D_s = D/W^{1/p}$ = scaled apparent crater depth, pth root scaling, $ft/(kt)^{1/p}$.

Further, let us define the following terms:

Z_w = actual depth of burial for a charge of weight W,

R_w = actual crater radius for a crater made with a charge of weight W,

D_w = actual crater depth for a crater made with a charge of weight W.

Method of Analysis

The relationships between crater radius and depth and depth of burst for any charge weight W can be expressed as:

$$R_w = f_r(Z_w), \tag{1}$$

$$D_w = f_d(Z_w). \tag{2}$$

Using data taken at one charge weight, W_1, it is possible to determine the form of (1) and (2) without any assumptions regarding scaling laws.

If we assume that an independent empirical scaling law exists for each

dimension, for a crater produced with a charge weight W_2 whose radius and depth are R_{w_2} and D_{w_2}, respectively, we can write

$$R_{w_2} = R_{w_1} \left(\frac{W_2}{W_1} \right)^{1/p_r}, \tag{3}$$

$$D_{w_2} = D_{w_1} \left(\frac{W_2}{W_1} \right)^{1/p_d}, \tag{4}$$

$$Z_{w_2} = Z_{w_1} \left(\frac{W_2}{W_1} \right)^{1/p_z}. \tag{5}$$

If, for example, one knows p_z, Z_{w_1} can be calculated from (5) which allows determination from (1) and (2), of R_{w_1} and D_{w_1}.

These parameters, in turn, permit calculation of p_r and p_d. Unfortunately, there are three independent parameters in the system and only two equations. Thus, an additional relationship is necessary to this system of equations.

A dimensional analysis of the cratering problem by Chabai,[16] in which consideration is given to such factors as gravity, overburden pressure, and the internal frictional forces of the medium, leads to a somewhat complicated set of conditions which must be observed to assure complete similarity. However, one of the simpler conditions requires that the depth of burst be proportional to the crater dimensions. If we modify this condition slightly to require that the depth of burst be proportional to either the radius or depth, depending on which quantity is under consideration, we have an additional relationship that will allow solution of the problem. This assumption would appear to be reasonable and should not restrict the freedom of the analysis to any appreciable degree. This is especially true in view of the rather small values of df_r/dZ and df_d/dZ over most of the range of interest. Thus we can write

$$R_{w_1} = R_{w_2} \left(Z_{w_1} / Z_{w_2} \right) = \beta_r Z_{w_1}, \tag{6}$$

$$D_{w_1} = D_{w_2} \left(Z_{w_1} / Z_{w_2} \right) = \beta_d Z_{w_1}, \tag{7}$$

where

$$\beta_r = R_{w_2}/Z_{w_2},$$

$$\beta_d = D_{w_2}/Z_{w_2}.$$

From (1) and (2) we have

$$R_{w_1} = f_r\left(Z_{w_1}\right), \tag{8}$$

$$D_{w_1} = f_d\left(Z_{w_1}\right). \tag{9}$$

Eliminating R_{w_1} and D_{w_1} we have

$$\beta_r Z_{w_1} = f_r\left(Z_{w_1}\right), \tag{10}$$

$$\beta_d Z_{w_1} = f_d\left(Z_{w_1}\right). \tag{11}$$

By finding the roots of these equations we can determine the equivalent depth of burst Z_{w_1} for a charge W_1 which corresponds to the actual depth of burst Z_{w_2}. Knowing Z_{w_1} and Z_{w_2}, we can find the value of p_z that satisfies these conditions from (5). Since both (10) and (11) lead to an independent value for p_z, it is possible, from each crater made with a charge of weight W_2, to obtain two values for the empirical scaling constants, p_r and p_d.

If W_1 and W_2 are two different types of explosive, the cratering efficiency of one relative to the other ϵ, may be obtained by rewriting (5) so that we have

$$Z_{w_2} = Z_{w_1}\left(\frac{\epsilon W_2}{W_1}\right)^{1/p_z} \tag{12}$$

If it is assumed that the value of p_z is known, the values of ϵ can be found by the same procedure that was used to calculate p_r and p_d above. Again we will have two values for the efficiency ϵ_r and ϵ_d.

Calculation of Empirical Scaling Law

From the 256-lb data given in Appendix A, an analytical fit for (1) and (2) has been derived. Initial attempts to fit these data with ordinary least-squares polynomial fits led to unsatisfactory results. In an attempt to get

better analytical fits, constraints were imposed on the data. It was obvious that the data in the region of shallow depths of burst were quite linear. Using a suggestion by M. Moravcsik, this portion of the curve was constrained to have zero curvature by inverting all the data through a single point on the ordinate and fitting both the original points and the inverted points with a single curve. The inversion point was determined by making a linear fit to the data at shallow depths of burst and calculating its intersection with the y axis. Thus, if this point is designated $(0, y_o)$, for each data point (x, y) an additional data point at $(-x, 2y_o - y)$ is added and both sets of points are fitted with the same curve. This results in a curve that is antisymmetrical about the inversion point. Least-squares fits by this method, of course, yield only odd-powered polynomials (plus a constant term).

An additional constraint was the recognition of the fact that for depths of burst beyond a certain point no significant crater will be produced. If data are taken beyond this point, any fit will attempt to go through the middle of such data, whereas the deepest significant data point is the shallowest depth of burst that would result in no crater. Therefore, to minimize this uncertainty, the data from the four deepest depths of burst were omitted from the fits even though they are presented with the data.

Using this process it was possible to make a satisfactory least-squares fit to the 256-lb data with a simple power series expansion. Fifth-order fits were sufficient to represent both radius and depth and are as follows:

$$R_{256} = 8.044 + (7.550 \times 10^{-1})\, Z_{256} - (1.878 \times 10^{-3})\, Z_{256}^3 - (3.485 \times 10^{-7})\, Z_{256}^5, \qquad (13)$$

$$D_{256} = 2.337 + (8.507 \times 10^{-1})\, Z_{256} - (4.937 \times 10^{-3})\, Z_{256}^3 + (6.827 \times 10^{-6})\, Z_{256}^5. \qquad (14)$$

A plot of the 256-lb data along with these fits is shown in Fig. 16. Also shown in Fig. 16 is the percent standard deviation calculated for these fits. For most of the region of interest the standard deviation of the radius curve is approximately 5%, deviating from this figure only for depths of burst greater than 14 ft. The percentage error of the depth curve is approximately the same, being about 5% for depths of burst less than 10 ft, but increases rather rapidly for larger depths of burst to 10% at 15 ft.

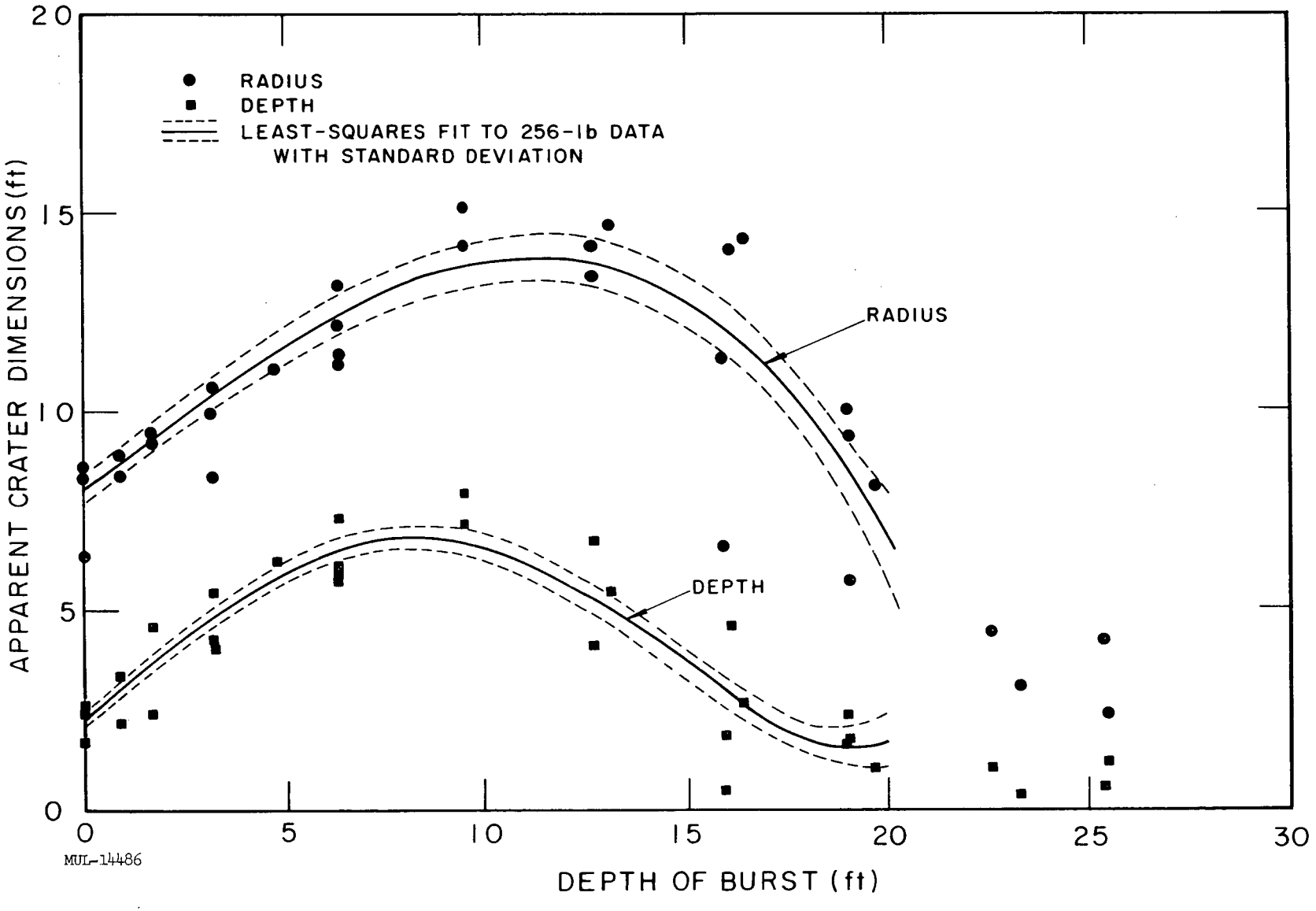

Fig. 16. Crater dimensions vs depth of burst for 256-lb H. E. shots in NTS alluvium.

With the expressions in (13) and (14) for f_r and f_d, the 40,000-lb data (W_2 = 0.02 kt) listed in Appendix A can be used to calculate values for the scaling exponent p. Determining the roots of the fifth-order function by iteration, we find the following values for p:

Shot	Depth (ft)	p_r	p_d	$\bar{p}$
Jangle H.E.-2	5.1	3.43	3.33	3.38
Stagecoach 2	17.1	3.25	3.41	3.33
Stagecoach 3	34.2	3.35	3.48	3.42
Stagecoach 1	80.0	3.18	3.38	3.28
Average		3.30 ± 0.10	3.40 ± 0.05	3.35 ± 0.09

The uncertainties on the average values are observed standard deviations.

Thus, we find that comparison of the 256-lb and 40,000-lb data leads to a $W^{1/3.3}$ scaling for radius and $W^{1/3.4}$ scaling for depth. However, considering the standard deviation it would probably be better, based on this data alone, to use $W^{1/3.35}$ scaling for both radius and depth. The effect of depth of burst does not appear to be consistent, and the only conclusion is that within the scatter of the data there is no discernible effect.

Analysis of the errors involved in the calculation of p leads to the following expression:

$$dp_r = \frac{p_r^2}{\ln (W_2 / W_1)} \left(\frac{df_r}{f_r} + \frac{dR_{w_2}}{R_{w_2}} \right), \qquad (15)$$

where df_r/f_r is the probable error associated with the least-squares fit of the W_1 data, and dR_{w_2}/R_{w_2} is the probable error in the observed crater dimension, assumed to be ± 5%.

A similar expression will hold for dp_d. Substitution of the appropriate values into (15) leads to a predicted error of about ± 0.13 in the values of p_r and p_d, which is about 1.5-2 times the observed standard deviations.

A similar treatment of the 2560-lb data does not lead to meaningful results. Values for p range from 2.8 to 5.3. This range in the values for p is so wide as to lead one to the conclusion that the large scatter of 2560-lb cratering data combined with the small yield range from 256 to 2560-lb is not adequate to allow determination of scaling exponents.

Application of the above analysis to the data from the Scooter detonation leads to:

$$p_r = 3.42 \pm 0.09,$$
$$p_d = 3.38 \pm 0.09,$$
$$\bar{p} = 3.40 \pm 0.09.$$

Averaging the data from these five craters we arrive at the following result:

$$\bar{p}_r = 3.33 \pm 0.10,$$
$$\bar{p}_d = 3.40 \pm 0.05,$$
$$\bar{p} = 3.36 \pm 0.08.$$

The uncertainties are the observed standard deviations, and it can be seen that they fall well within the probable error of the calculation. It is interesting to note that the average value for $\bar{p}_r$ is below the average value of $\bar{p}_d$. From consideration of the factors that are involved in the change in the scaling law, one would expect that p_d would approach 4 faster than p_r, although the rate is not known at the present time. However, it should also be noted that when the errors are considered, the difference between $\bar{p}_d$ and $\bar{p}_r$ is not statistically significant. Therefore the value of $\bar{p} = 3.36 \pm 0.08$ would appear to be the best value to use for further analysis. This value agrees quite well with the value derived by Chabai;[16] however, I believe this approach is much more straightforward than Chabai's and results in a plausible fit to the data with a much smaller probable error.

Nuclear and High Explosive Efficiencies

We can now calculate a value for the efficiency of nuclear explosives relative to high explosives by using the above value for $\bar{p}$ and the data from the nuclear and high-explosive craters. Following the above-indicated procedure, we obtain for the subsurface nuclear explosion:

Shot	Z(ft)	ϵ_r(%)	ϵ_d(%)	ϵ_v(%)*
Jangle U	17	87 ± 22	135 ± 22	103 ± 22
Teapot ESS	67	49 ± 20	132 ± 22	68 ± 22
Average		68 ± 15	134 ± 15	85 ± 15

* Volume efficiencies have been estimated only.

The difference between ϵ_r and ϵ_d is statistically significant and undoubtedly is related to the mechanisms of crater formation and the differences between nuclear and high explosives. Mechanisms dominant

in determining crater depth are not necessarily dominant also in determining crater radius. It is, therefore, not unreasonable that changes in the physical nature of the explosive could produce different effects on radius or depth. This subject will be explored at greater length in the later section on cratering mechanisms.

Calculation of the volume efficiency factor by comparison of crater volumes has not been done, but ϵ_v has been estimated from the volume for ϵ_r and ϵ_d, recognizing that the crater volume is proportional to R^2D. The difference in this efficiency for the two nuclear craters is, of course, directly attributable to the differences in the ϵ_r. This difference may be due to the difference in emplacement conditions, the Teapot ESS shot being close-tamped while the Jangle U shot was detonated in a room which, if spherical, would have a radius of about 6 ft.

Efficiencies for the Jangle S surface shot have not been included in the above discussion because of the tremendous differences in the phenomena. However, they can be simply calculated using (13) and (14) and a value for p of 3.36. This gives the result that $\epsilon_r = 3.5 \pm 0.1\%$ and $\epsilon_d = 17 \pm 1\%$; ϵ_v is estimated to be $6 \pm 1\%$. These low efficiencies, reflecting the large proportion of the energy which is lost from a surface nuclear explosion, demonstrate that surface detonation is extremely inefficient for nuclear excavation.

Based on the above average efficiency values for dimensions of craters produced by subsurface detonations, radii and depths of nuclear craters would be expected to be about 90% and 110%, respectively, of the corresponding dimensions for high-explosive craters produced under similar conditions. For practical purposes it would appear reasonable for craters produced by subsurface nuclear explosions, to use an efficiency of 100% with suitable standard deviation.

Summary

The scaling law derived above has been rounded to the significant figures, and for the rest of this paper it will be assumed that crater dimensions scale by the following scaling laws:

$$R = R_s W^{1/3.4},$$

$$D = D_s W^{1/3.4},$$

$$Z = Z_s W^{1/3.4}.$$

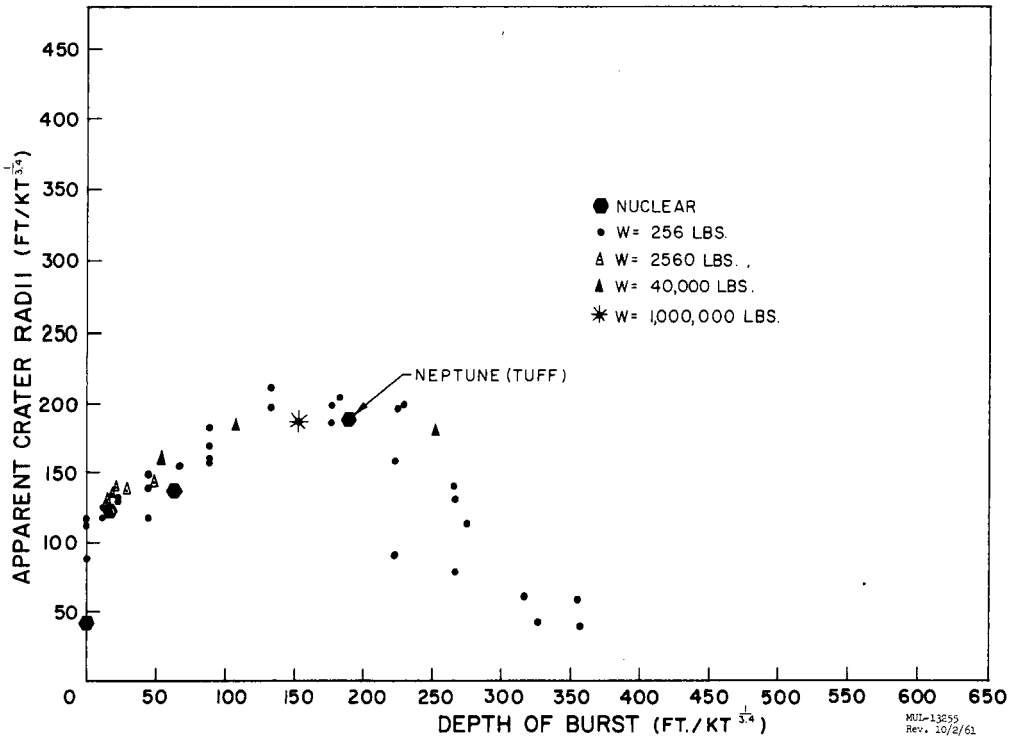

Fig. 17. Apparent crater radius vs depth of burst for NTS alluvium, including all available data ($W^{1/3.4}$ scaling).

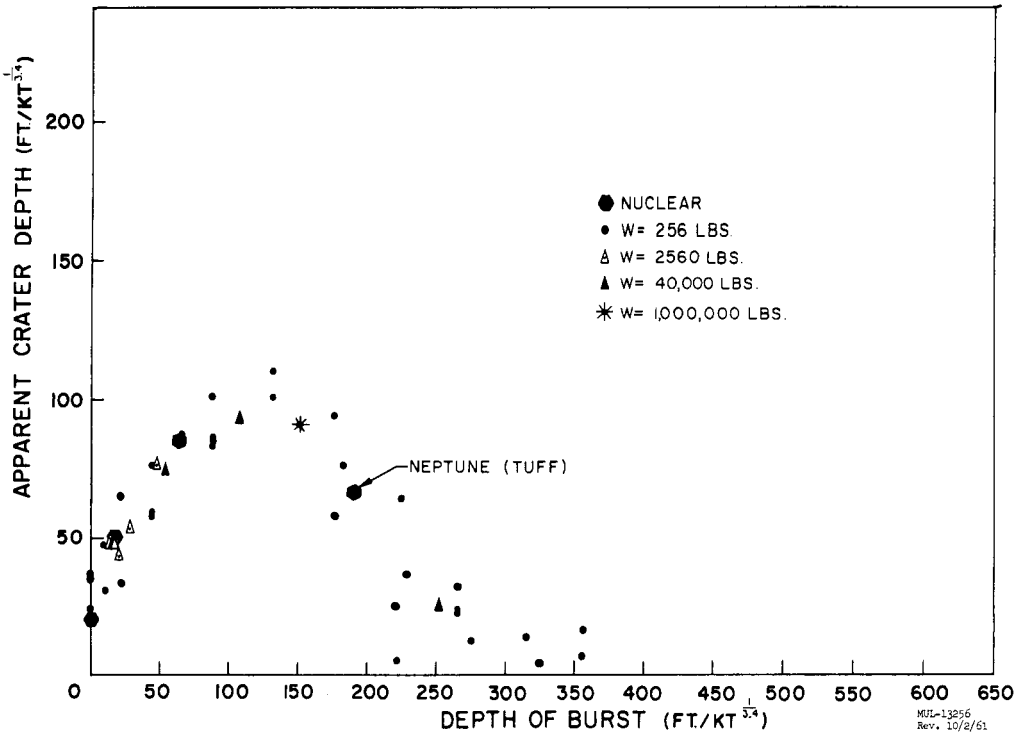

Fig. 18. Apparent crater depth vs depth of burst for NTS alluvium, including all available data ($W^{1/3.4}$ scaling).

All of the NTS desert alluvium data listed in Appendix A have been plotted using this scaling law and are shown in Figs. 17 and 18. The least-squares fits given in (13) and (14), when scaled to 1 kt by $W^{1/3.4}$, have the form:

$$R_s = 112.5 + (7.55 \times 10^{-1})\, Z_s - (9.6 \times 10^{-6})\, Z_s^3 - (9.11 \times 10^{-12})\, Z_s^5,$$

$$D_s = 32.7 + (8.51 \times 10^{-1})\, Z_s - (2.52 \times 10^{-5})\, Z_s^3 + (1.78 \times 10^{-10})\, Z_s^5.$$

These equations are plotted in Fig. 19. In Fig. 20 are plotted the observed standard deviations of these equations as a function of depth of burst, Z_s.

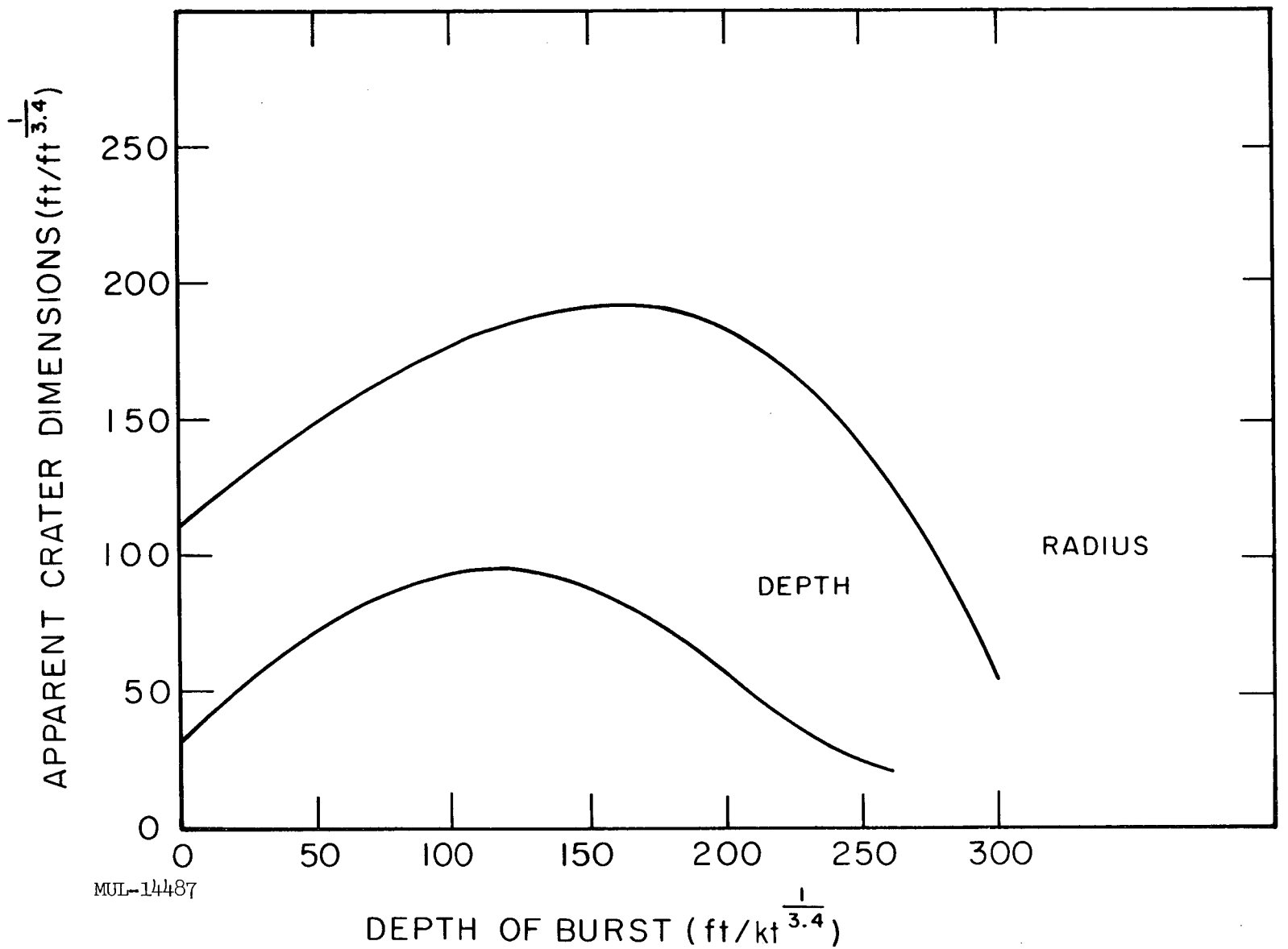

Fig. 19. Apparent crater dimensions vs depth of burst for NTS alluvium, showing the curves that were fitted to the data by least squares. Data are from H. E. craters, and are scaled by $W^{1/3.4}$.

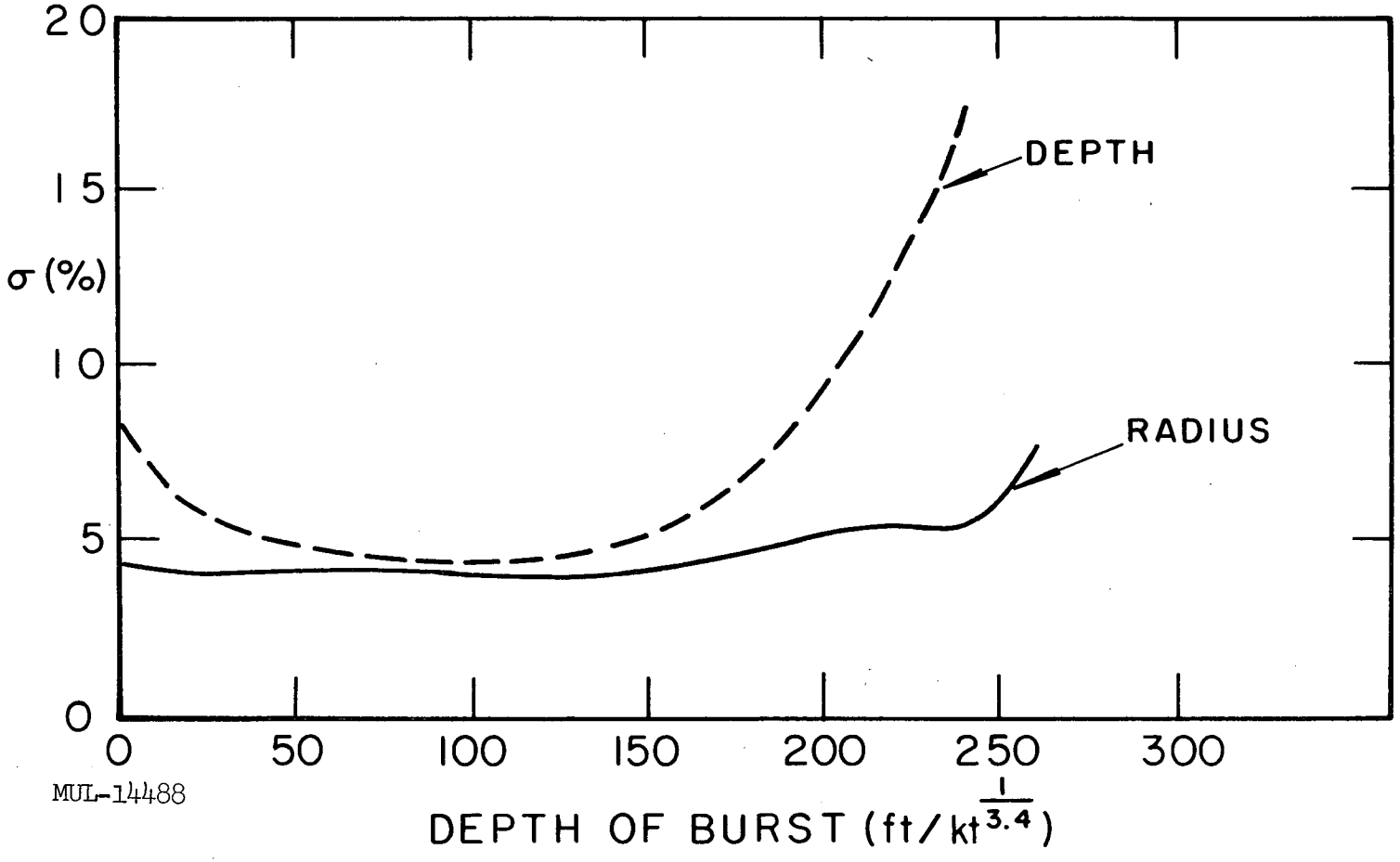

Fig. 20. Percent standard deviation of NTS alluvium data from least-squares-fitted curves, plotted as a function of scaled depth of burst ($W^{1/3.4}$ scaling).

CHAPTER V. PRELIMINARY THEORY OF CRATER FORMATION

Much of the past work on the mechanics of crater formation has been of a qualitative nature, with a few notable successes for quantitative analysis of isolated phases of the processes involved. Most of the analysis has been based upon empirical relationships or dimensional analysis arguments which, while providing a useful bridge, have not given much insight into the basic problems involved. This report does not present a quantitative discussion either, but will, I hope, set forth a few ideas relating to the mechanisms involved in the formation of explosive craters, with some estimates of their relative orders of magnitude. Because of the rather strong current interest in impact craters and the theories of meteoritic origin for the lunar craters, I have devoted a small amount of discussion to this subject. However, the analogy between explosive craters and impact craters is not complete, and I will attempt to point out some of the differences.

The ideas expressed in this document are based on many sources, ranging from the experimental data derived from cratering programs such as Teapot ESS,[18] Scooter, Bureau of Mines[1] work, and Neptune re-entry and reconstruction,[20] to theoretical advances made possible through the development of machine calculations such as the UNEC code described elsewhere by Maenchen and Nuckolls.[36]

Mechanisms of Crater Formation

One phenomenon that is present in all underground explosions to varying degrees is the crushing, compaction, and plastic deformation of the medium immediately surrounding the source of the explosion, whether it be a chemical, nuclear, or impact explosion. As the high pressure gases generated by the explosion push on the walls of the cavity, a shock wave is generated which is characterized by a spherical surface across which there is a sharp discontinuity in the physical state of the material. This discontinuity propagates outward at a velocity which, for high pressures, is faster than the speed of sound in the medium. For chemical explosives the initial pressures are of the order of 100-200 thousand atmospheres; for a nuclear explosive they are as large as 10-100 million atmospheres, depending on the initial cavity size; and for a meteor impact explosion they can have

any value ranging between these two, depending on the meteor velocity and the type of material which it hits. For extremely high pressure explosions where pressures are greater than about 500 thousand atmospheres, the medium is melted and vaporized when the shock passes through it. As the shock wave moves outward in a spherically diverging shell, the peak pressure in the shock front drops because of spherical divergence as well as energy expenditure in doing work on the medium. For pressures above the dynamic crushing strength of the material this work appears in the form of crushing, heating, and physical displacement. In regions outside this limit the shock wave will still produce permanent deformation by plastic flow until the peak pressure in the shock front has decreased to a value equal to the plastic limit for the medium. This plastic limit marks the boundary between the elastic and plastic zones described for Fig. 1. As with the definitions given for Fig. 1, the limits of crushing and plastic deformation vary widely from material to material.

The above picture of the first few milliseconds of an explosion neglects the effects of any free surface, effects which are exceedingly important. As a compressive wave encounters a free surface, it must match the boundary condition that the pressure, or more correctly the normal stress, be zero at all times. This results in the generation of a negative stress wave or rarefaction which propagates back into the medium. The process is shown schematically in Fig. 21, where for simplicity a triangular-shaped stress wave, $\sigma_n(t)$, has been assumed instead of the more appropriate exponential shape. At some depth, such as P in Fig. 21, the sum of the two stress waves equals the dynamic tensile strength of the medium. The medium breaks in tension at P and a piece flies off with a velocity characteristic of the total momentum trapped in it. This produces a new free surface that will break at P_1, and again at P_2. For a loose material like alluvium, this process (called "spall") makes almost every particle fly into the air individually, whereas in a rock such as basalt the thickness of the slabs is generally determined by presence of pre-existing joints and zones of weakness. For the case of a small sample or where there is a very massive block, the dynamic tensile strength of the rock determines the thickness of spall. As the distance from the explosive to the free surface increases, the peak pressure decreases and so the maximum possible tensile stress

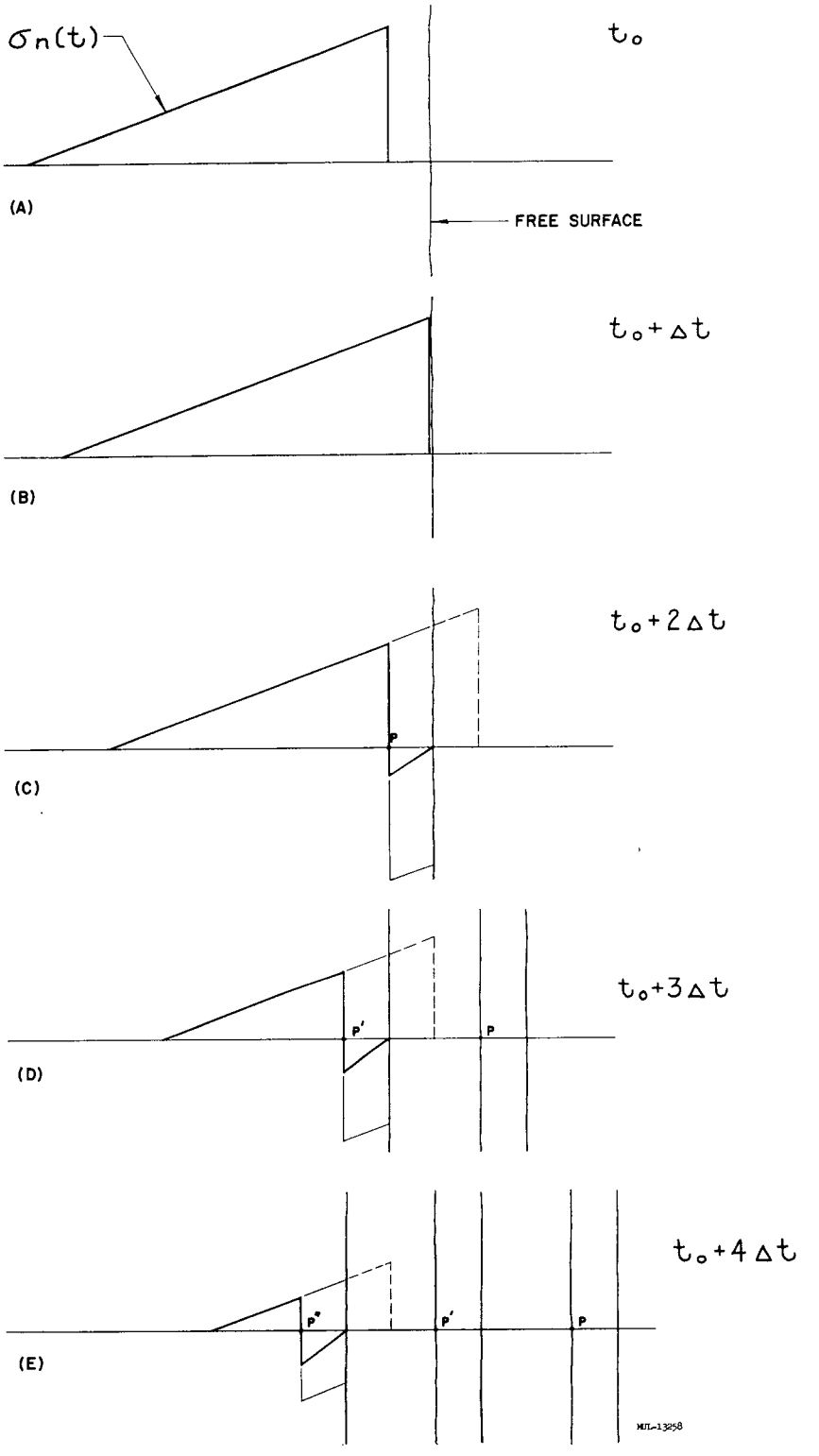

Fig. 21. Schematic drawing illustrating the spall mechanism.

decreases until it no longer exceeds the tensile strength of the medium. In addition, the velocity given to the spall decreases in proportion to the peak pressure.

For ranges beyond the point where spall occurs, the negative stress in the rarefaction wave will decrease the shear strength of the medium, which results in large plastic deformations and ruptures. This makes the rupture zone extend a considerable distance along the surface and contributes to the formation at the lip. Ultimately, the surface expression of a deep underground explosion is only a small elastic excursion of the surface. Spalling of the free surface is one of the most important phenomena in cratering, especially for shallow depths of burst, and is the easiest mechanism to observe and to calculate.

The third mechanism of importance in cratering, particularly for deeper craters, is what I have termed "gas acceleration." This is a long-period acceleration given the material above the explosion by the adiabatic expansion of the gases trapped in the cavity. For some cases, particularly for deep depths of burst, this gas also gives appreciable acceleration during its escape through cracks extending from the cavity to the surface. For very shallow depths of burst the spall velocities are so high that the gases are unable to exert any pressure before venting occurs. For very deep explosions, the acceleration given the overlying material is so small as to be negligible. This process will be examined in more detail in a later section.

Subsidence is the fourth major process that makes a significant contribution to the formation of the apparent crater. It is very closely linked to the first process of compaction and plastic deformation, without which there would be no void into which material could subside. Subsidence occurs when the spall or gas acceleration has so distended the overlying material that large cracks are produced through which the explosion gases escape. The overlying material, having been fractured and crushed by the shock wave, collapses into the cavity. Subsidence is most important, of course, for very deep explosions.

Effects of Depth of Burst

The part each of the above mechanisms plays in producing a crater

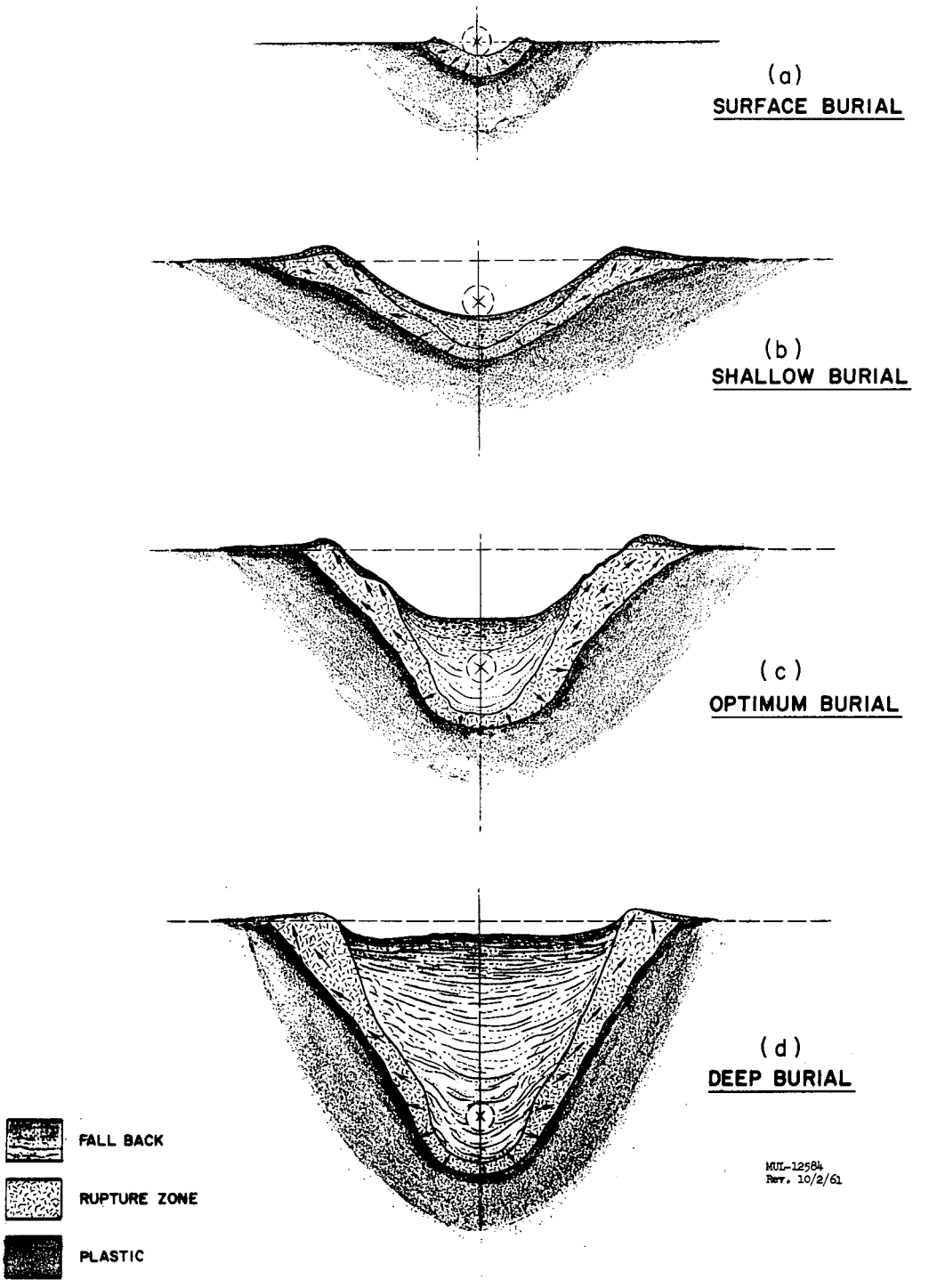

Fig. 22. Typical crater profiles vs depth of burst for alluvium.

is very strongly dependent on the scaled depth of burst of the explosion. Shown in Fig. 22 are typical crater cross sections based on the above alluvium data, showing the extent of the various zones. These figures will be used to depict the role each mechanism plays in producing a crater. The small dashed circle about the detonation point indicates the size of the original TNT sphere.

Surface burial. Figure 22a shows the crater resulting from the detonation of an explosive very near the surface of the ground. As can be seen, the crater is produced to a large degree by compaction and plastic deformation. There is scouring action by the gases in the initial gas sphere which erodes the surface of the crater, but this is not a significant mechanism in the formation of the crater. The radius is extended to its limit by spalling action resulting from a horizontally diverging shock wave, but the major process for the depth of the center and for lip formation is the plastic deformation and flow of the material in the rupture zone. Very little fallback is found in a crater of this kind, and the true crater and apparent crater are almost the same.

The picture shown in Fig. 22a is based on data from the nuclear crater Jangle S, which has dimensions somewhat smaller than would be expected from a chemical explosion at the same depth of burst because a large fraction of the energy from a nuclear explosion is released in the form of thermal and x-ray radiation. A meteoritic impact explosion could be considered analogous to a surface burial only for very low velocity meteors, in which case the pressures involved would be more like those occurring in a chemical explosion than a nuclear explosion, with the result that dimensions more like those shown in Fig. 22a for a surface burst would be expected. However, the mechanisms involved would be essentially the same as for the surface nuclear explosion.

Shallow burial. A cross section of the crater resulting from shallow burial of the explosive is shown in Fig. 22b. This scaled depth of burst corresponds roughly to the scaled depth of the nuclear explosion Teapot ESS (66 ft). Spalling of the free surface has now become the dominant process for the formation of the crater. Gas acceleration and scouring action are of only minor importance because of the high velocities given to the material by the spalling process. The radius of the crater is determined

by the limit of the spalling process, whose velocities decrease rather rapidly with increasing surface radius. This decrease of spall velocity with radius leads to the "folding back" of the material on the edge of the crater to form the lip that is evident in many craters including Teapot ESS and Meteor Crater, Arizona, noted by Shoemaker.[5] The maximum radius of the spalling process decreases as one goes below the original surface because of the increased total path length which the shock and the rarefaction must travel. This results in a roughly parabolic-shaped true crater. The extent of the fallback and rupture zone for a crater from a shallow depth of burst were very well defined by the sand column techniques used on Teapot, and Fig. 22b is based very closely on this work.

The impact and explosion of a high velocity meteor is probably most closely simulated by a nuclear explosion at a shallow depth of burial. For example, Shoemaker's analysis[5] suggests that Meteor Crater corresponds to an explosive-produced crater with scaled depth of burst of about 45 feet. Further, most of the general features noted in meteor craters are found in explosion craters for shallow scaled depths of burst. A nuclear explosion would more closely simulate the meteor impact explosion than would chemical explosions, because of the very high initial pressures and energy densities which are found in both nuclear and meteor explosions. Both are characterized by relatively small amounts of condensable explosion products and by vaporization of considerable quantities of the medium surrounding the explosion. However, experience has shown that for nuclear explosions buried at shallow depths in alluvium, there are very small differences between chemical explosive and nuclear explosive craters. This is believed to be because (1) gas acceleration is not important for shallow depth of burst, and (2) there is 10-20% water in the alluvium, which when vaporized produces gases in the cavity that are noncondensable at moderate temperatures. Condensable gases, i.e., gases that condense at a relatively high temperature, such as silica vapor, drop out of the vapor phase relatively early in the expansion and do not contribute to the gas pressure in the cavity. Water vapor and CO_2 do not condense and hence add to the gas phase.

The virtually complete venting of the radioactive material from the Teapot ESS explosion leads one to the conclusion that, if the high pressures and temperatures predicted for Meteor Crater by Shoemaker are correct,

the meteoritic material from a meteor impact would also be completely vaporized, vented to the atmosphere, and spread over the surrounding countryside. One should add that there is undoubtedly not an exact correlation between an impact crater and an explosive crater because the meteor's energy is released in the form of a line source as opposed to a point source for an explosion. Thus, some deviation from the dimensions predicted for explosion craters should be expected.

Optimum burial. For an explosion at optimum depth of burial, i.e., at a depth that results in maximum apparent crater dimensions, the resulting crater would appear as shown in Fig. 22c. The apparent crater dimensions shown are taken from the Scooter crater. The true crater and rupture zone for both this sketch and for the deep burial (Fig. 22c) are only estimates, inasmuch as there were no postshot excavations. For craters at these depths of burst, all three phenomena—plastic deformation, spall, and gas acceleration—are important, but the latter has become the most prominent feature of the cratering process. When the shock wave reaches the surface, it has decayed to the point where, although it is still capable of fracturing the material in tension (since most media have very small tensile strengths), the velocities given the material are relatively small. Because the maximum height to which a particle will go is proportional to the square of the initial velocity, the throwout would not go any appreciable distance into the air if spalling were the only process.

The inadequacy of the spall mechanism and the necessity for some kind of gas acceleration is best seen from the surface motion data from Scooter obtained from high speed motion pictures of seven surface targets.[37] Taking the displacement-versus-time data and computing vertical velocities, we get the plots shown in Fig. 23. The straight lines are least-squares fits to the data over the ranges of 80-350 msec and above 350 msec. General venting which obscured the targets occurred at about 1.2 sec. As can be seen from Fig. 23, the data very easily can be broken down into these two regions, one with a negative acceleration and the other with an approximately uniform positive acceleration. The data from the graphs in Fig. 23 are summarized in Table IV where the initial velocities and the velocities at 1.2 sec are given, along with the accelerations derived from the slope of the lines in Fig. 23. In addition, the maximum heights to which a particle

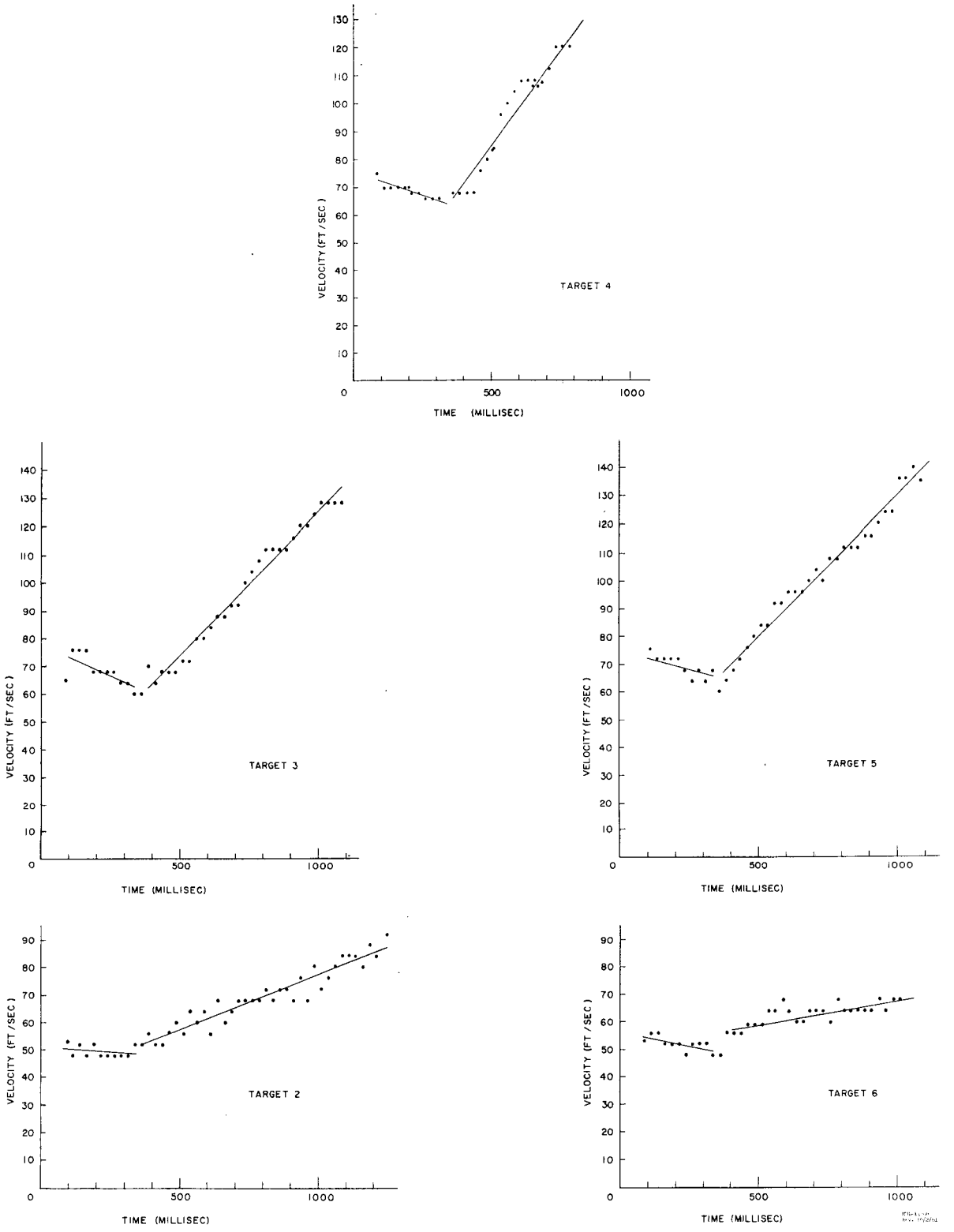

Fig. 23. Velocities of surface targets vs time, Project Scooter.

would go are computed for both the initial velocity and the 1.2-sec velocity, using the equation $h = v^2/2g$. Heights from the 1.2-sec velocities are quite consistent with observed particle trajectories, indicating that there was no appreciable acceleration after venting occurred.

Table IV. Summary of acceleration, velocity, and displacement data for Scooter surface targets.

Target Numbers	2	3	4	5	6
Distance from surface zero of target (ft)	60	30	0	30	60
Initial velocity (ft/sec)	50	74	73	73	54
Acceleration, 80-350 msec (ft/sec^2)	-8	-46	-34	-27	-20
Acceleration, 350-1200 msec (ft/sec^2)	+39	+102	+133	+100	+17
Velocity at 1.2 sec (ft/sec)	85	145	177	150	70
Maximum height from initial velocity (ft)	39	86	83	83	46
Maximum height from 1.2-sec velocity (ft)	106	328	490	352	77

The picture presented by these data is fairly clear. The first motion experienced by the surface of the ground is that produced by spall. The highest spall velocities of about 70-75 ft/sec are realized at surface zero, decreasing as one goes away from this point because of the increased travel length for the shock wave. As the rarefaction propagates back toward the cavity, all the material is given an upward velocity which decreases in magnitude with depth. After the passage of the shock, the material is in approximately free fall as shown by the magnitude of the negative acceleration in the period from 80-350 msec. When the rarefaction reaches the cavity, the cavity begins to expand very rapidly, pushing on the loose and broken layers above it, picking up each layer as it moves upward, bringing them all to the same velocity in much the same manner that an engine of a freight train accelerates its cars when it reverses direction. Ultimately this second push reaches the

surface and all the earth or rock above the explosion is moving as one mass. In Scooter, the hemispherical surface set in motion by spall experienced a relatively uniform positive acceleration starting at about 350-400 msec. The rate of acceleration was very dependent on the radial distance from surface zero. Finally, radial divergence of the hemispherical plug causes large cracks to open from the cavity to the surface, through which the high pressure gas escapes. During its escape, it gives appreciable acceleration to the material through which it is passing. This results in the surface layers experiencing a much longer period of acceleration than the deep layers. Much of the material immediately above the cavity does not attain the high velocity of the surface and falls back in place with very little mixing or disruption of the stratigraphy.

An order-of-magnitude estimate of the validity of this picture can be made, based on the results of a UNEC calculation[36] and some simple concepts. The UNEC code is a program for the IBM 7090 which can make a one-dimensional elastic-plastic-hydrodynamic calculation of the early history of an underground explosion. Calculations for Scooter give the result that the pressure of the gas in the cavity is approximately 175 bars at the time when the shock wave reaches the surface of the ground. The cavity radius is about 36 ft versus an initial radius of about 15 ft for the TNT sphere. The initial surface velocity predicted by UNEC is 103 ft sec, a number in fair agreement with the observed values of 70-75 ft sec. This agreement is particularly encouraging when one considers the difficulties of making an elastic-plastic calculation for a sand-gravel mixture.

Using these numbers, an estimate can be made of the magnitude of the gas acceleration by considering the material contained in the solid angle, Ω, above the cavity. This solid angle is defined by the approximately hemispherical surface which is the first evidence of surface motion. Figure 24a shows a sketch of the situation at 350 msec if the material above the cavity continues to move but the cavity remains at the 36-ft radius. Numerous voids are opened up whose total volume equals the volume of the hemispherical segment. Fig. 24b shows the configuration if the cavity is allowed to expand to take up all these voids. The new cavity volume is now $V_o + \Delta V$ where ΔV is the volume of the spherical segment. Thus

$$\Delta V = \frac{\pi h^2 (3R - h)}{3},$$

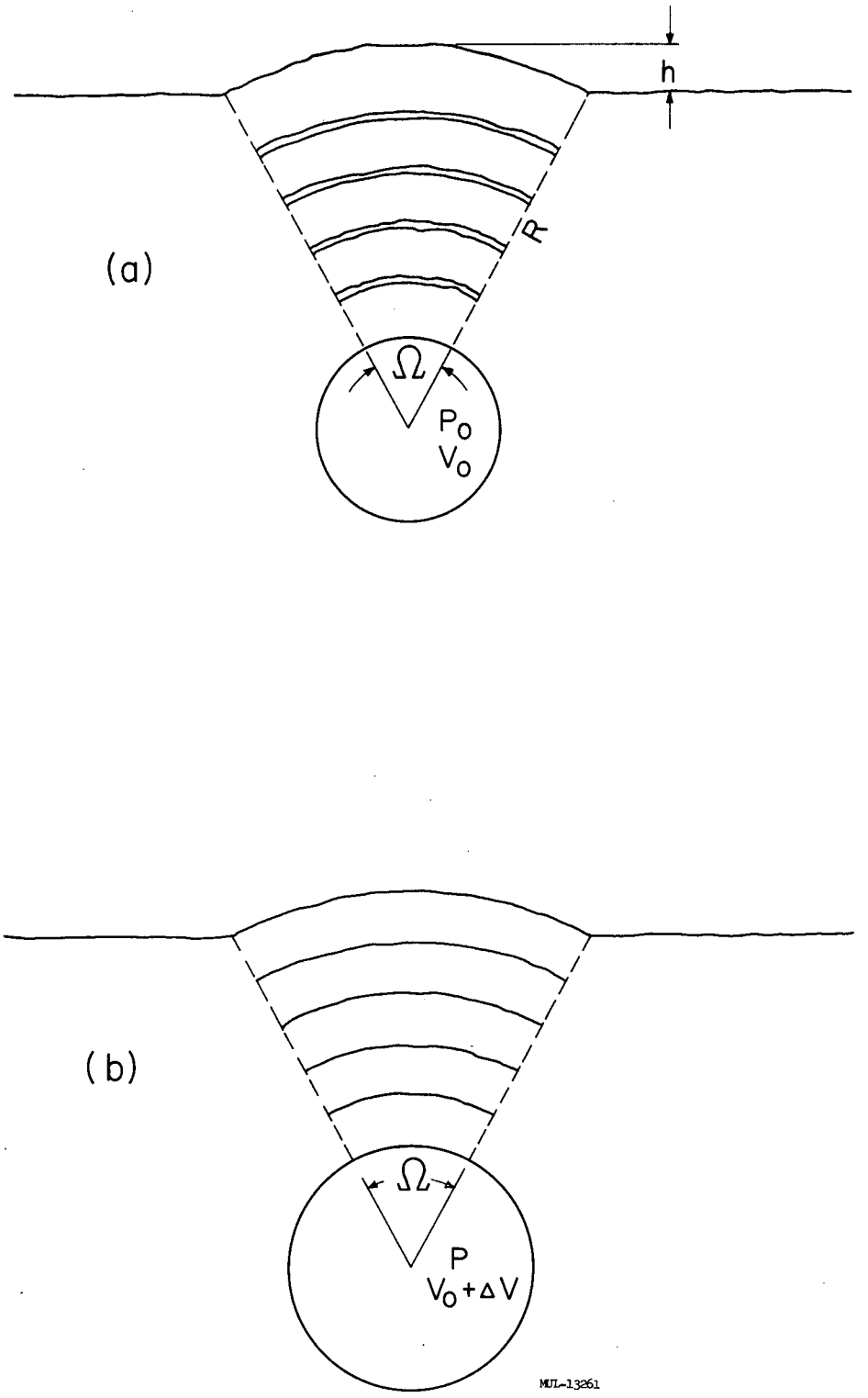

Fig. 24. Schematic drawing of optimum depth of burial for (a) no expansion of cavity, (b) cavity expanded to take up voids.

where R = radius of hemisphere = depth of burst + h, and h = height of hemispherical segment. The new pressure in the cavity after this adiabatic expansion is given by

$$P = P_o \left(\frac{V_o}{V_o + V_\Delta} \right)^\gamma ,$$

where P_o = original pressure in cavity.

If we now assume that this conical mass moves as one under the influence of the gas in the cavity, we have

$$PA = Ma$$

where

$$M = \text{mass of cone} = \frac{\Omega R^3 \rho}{3} ,$$

$$A = \text{area of the truncated cone} = \Omega \left(\frac{V_o + \Delta V}{4\pi/3} \right)^{2/3} ,$$

a = acceleration experienced by conical mass.

Thus we have

$$a = \frac{\Omega P_o \left(\frac{V_o}{V_o + \Delta V} \right)^\gamma \left(\frac{V_o + \Delta V}{4\pi/3} \right)^{2/3}}{\frac{R^3 \rho \Omega}{3}}$$

$$= 1.15 \frac{P_o (V_o + \Delta V)^{2/3}}{R^3 \rho} \left(\frac{V_o}{V_o + \Delta V} \right)^\gamma$$

At 350 msec the observed height of the spherical segment for Scooter was approximately 16 ft (490 cm). Using 125 ft (3810 cm) for the depth of burst, R = 4300 cm and

$$V_o = 5.55 \times 10^9 \text{ cm}^3,$$

$$\Delta V = 3.12 \times 10^9 \text{ cm}^3.$$

The density of alluvium is about 1.6 g/cm^3. The for TNT at 175 bars as obtained from Jones and Miller[38] is about 1.3. Using P_o = 175 bars = 1.75×10^8 dynes/cm^2, we have

$$a = 1.15 \times \frac{1.75 \times 10^8 (8.67 \times 10^9)^{2/3}}{1.6(4.3 \times 10^3)^3} \left(\frac{5.55}{8.67} \right)^{1/3}$$

$= 6.68 \times 10^3 (0.64)^{1.3} = 3.74 \times 10^3$ cm/sec^2
$= 123$ ft/sec^2.

Comparison of this number with the accelerations observed in Table IV for the period from 350-1200 msec shows that it is remarkably close to those observed, particularly for the central targets. It is considerably higher than observed accelerations of the targets 60 feet from the surface zero, even when one considers that the numbers given in Table IV are vertical components. One would not, of course, expect the acceleration to be constant in time, but to decrease with time because of the dropping pressures in the cavity. However, the continued acceleration of the surface layers by the gas escaping through cracks and fissures gives additional acceleration to compensate for this drop. Obviously, such a picture is inadequate, but it does indicate the correct order of magnitude of these effects.

The sequence and magnitude of events described above apply only to a medium such alluvium. For other media the numbers, and consequently the relative importance of the various mechanisms, may be greatly different. Some interesting information for another medium, basalt, is provided by preliminary results from high speed motion pictures of ground motion at surface zero for the three large Buckboard detonations. These 40,000-lb shots, designated shots 11, 12, and 13, were buried at depths of 25.5, 42.7, and 58.8 feet, respectively—corresponding to scaled depths of burst of 80, 135, and 186 feet, using $W^{1/3.4}$ scaling to 1 kiloton for ease of comparison with the alluvium data. The surface motion data for these three shots are given in Table V along with the spall velocities that were calculated by the UNEC code.

Table V. Surface motion data for Buckboard shots 11, 12, and 13.

Shot No.	11	12	13
Scaled depth of burst (ft)	80	135	186
Observed initial velocity (ft/sec)	330	150	120
Calculated initial velocity (ft/sec)	340	164	100
Residual cavity pressure (kilobars)	10	9	8

The agreement here is excellent. The higher velocities are attributable to the much greater strength and competence of the basalt. A shock wave is attenuated much less in traversing a foot of basalt than a foot of alluvium.

The result is that for a scaled depth of burst equal to Scooter's, the spall velocities are over twice as large in basalt as in alluvium. This means that the mechanics of cratering for an optimum depth of burial in basalt are much more like those for a shallow depth of burial in alluvium. The gas acceleration has little chance to accelerate the rock, and the crater is formed almost entirely by spalling. For deep depths of burial in basalt the spall velocity is not so high, but the mass of material to be accelerated by the gas is so large that the acceleration would be very small.

When considering impact crater mechanisms, it is obvious that gas acceleration must play a much less significant role because of the hole produced by the entry and explosion of the meteor. By the time gas acceleration would be important, this hole would be many times larger than the original size of the meteor because the hole made by the meteor acts as a linear energy source, expanding in a lateral direction under the influence of the cylindrical shock which is generated. Thus, this hole would not permit entrapment of the gases produced by the explosion. There has been a small amount of work done on the effects of the stemming of a cratering charge,[39] all at relatively shallow depths of burst. This work indicates that apparent crater dimensions are reduced by something like 15-30% by eliminating stemming; it contains no data on the effect of stemming at depths of burst near optimum, where the effect of gas acceleration would be most important, although it does show that the effect of stemming increases with depth of burst.

Deep burial. Figure 22d depicts the cross section of a crater resulting from the detonation of an explosive at a depth well beyond the optimum depth of burial. The apparent crater profile here follows closely the deepest Stagecoach crater, whose scaled depth was 253 ft. The spall velocities are now very small, about 10-15 ft/sec. The direct gas acceleration is almost an order of magnitude smaller than for optimum depth and is in general difficult to identify. The acceleration resulting from frictional drag by the escaping gases is probably most important for this situation. The fallback within the crater should be well ordered with little or no disruption of the stratigraphy, as indicated in the sketch. The lips are produced, to a very large extent, by the rupture and plastic flow of the material in the rupture zone. About 50-75% of the apparent crater volume can be attributed to subsidence, depending on the depth of burst.

Analysis of Neptune Crater

Based on the above picture, an analysis of the Neptune detonation described earlier has been undertaken to try to explain the observed phenomena. Using a postshot geological study of the regions surrounding the detonation point,[20] core holes drilled into the active region, and machine calculations of the expected behavior of underground detonations, it has been possible to reconstruct a history of the Neptune event, including the mechanisms that led to formation of the crater.

A few microseconds after detonation of the device, all of the material surrounding the device was vaporized and the mixture of hot air and vaporized material had filled the shot room. Since the volume of the room was approximately 5.8×10^7 cm^3 and there was about 10^6 g of material in the room (assuming the concrete floor was one face of the room), the gas would be at a temperature of about 150,000°K and a pressure of 25,000 atmospheres (bars). At these temperatures, the gas would be only partially ionized.* The radiation pressure is completely negligible. The 25-kilobar pressure in the room would not generate a shock strong enough to melt of vaporize the surrounding rock, but the shock would crush and fracture the tuff, permanently displacing the material near the room and allowing the cavity to expand. The high temperature gas in the cavity would vaporize and melt the inner surface of the spherical cavity by conduction, producing a thin molten lining. Such a picture is confirmed by samples of the fused material recovered from the Neptune area, which show that it occurs only as thin layers, a fraction of an inch thick, in contrast to the fused material from Rainier,[21] which was about a foot thick.

As the shock wave traveled outward, it decreased in strength, ultimately propagating as an elastic wave. The shock wave reached the sloping face of the mesa, which is 100 ft from the device, at about 12 milliseconds after the detonation. The rarefaction from the free surface, traveling back to the cavity at close to sonic speed, reached the liquid-lined sphere at about 25 milliseconds.

* The above temperatures and pressures are estimated on the basis of a Thomas-Fermi-Dirac equation of state for the material in the room. This equation of state is felt to be quite reasonable at these temperatures and pressures.

The initial spall velocity of the surface material as measured on Neptune near the region of maximum rupture was 30-40 feet/sec.[40] If it is assumed that these pieces moved from then on in free fall paths, under the influence of gravity alone, they would go only 15-25 ft in the air. Since large rocks were observed going much higher, it is clear that some sort of late-time gas acceleration occurred. Expansion of the cavity after the arrival of the rarefaction was followed by the outward rush of hot gases from the gas bubble, which accelerated the upward flight of the broken rock fragments, blowing them out of the crater. Venting occurred through cracks in the overlying strata with no general upheaval or mixing of the strata above the cavity, as evidenced by the clear delineation of the preshot geologic structure.[20]

Due to the low overburden pressure in the region of the Neptune detonation and the large gradient in the overburden pressure horizontally in the direction of the face of the mesa, the cavity expanded asymmetrically. Fractures extending large distances from the cavity were formed and hot gases penetrated them, producing fused layers of rock on the surface of the cracks. This resulted in traces of radioactivity throughout the region surrounding the cavity. Such widespread distribution of the radioactivity and heat from the detonation have made determination of the final cavity radii very difficult. Significant amounts of radioactivity have been found up to 30 ft from the detonation in the direction away from the face of the mesa and up to 50 ft toward the face. In general, the zones of maximum radioactivity define a maximum radius for the cavity of 15-20 ft. The large amount of radioactivity found up to 50 ft away in the direction of the face of the mesa is probably due to early venting of the cavity along bedding planes in that direction. This is indicated by films that show venting from the surface of the slope occurring at a point well below the point of maximum rupture, before the venting at the point of maximum rupture is visible.

Following the venting and collapse of the cavity, a chimney or subsidence was formed which propagated to the surface. If all of the volume of the cavity had been communicated to the surface by the chimney, it would have contributed approximately 640 yd^3 to the apparent crater's volume 22,000 yd^3.

Summary

In an attempt to give an overall picture of the effects of these four

mechanisms and their relative importance at various depths of burst, I have constructed a schematic diagram showing their effect on one crater dimension. For the purpose of this example I have chosen to use apparent crater depth because the role played by each mechanism is comparatively simple. Figure 25 shows, in a dimensionless graph, these relationships. The contribution from compaction and plastic deformation and subsequent subsidence is a maximum for a surface detonation and decreases somewhat asymptotically with depth because of the increasing overburden pressure. The contribution of spall to apparent crater depth is, more or less, directly proportional to the depth of burst for shallow depths of burst; it peaks and then decreases as shown for larger depths of burst because of the decrease in surface velocities. The effects of gas acceleration do not become significant until the contribution from spalling starts to decrease. They then increase somewhat to a peak, and tail off as shown. The effectiveness of even this tail is dramatically illustrated by films of the Blanca nuclear event,[21] an event somewhat similar in geometry to Neptune but with a scaled depth of burst about 50% greater. The surface spall created no crater at all for this shot. However, a large cavity or camouflet was produced which collapsed, with the subsidence progressing toward the surface. This collapse required 15 seconds before it reached the surface, at which time the gases trapped in the cavity vented to the surface with a very startling plume of gas which went about 600 ft in the air. When this venting first evidenced itself, some of the large surface rocks were ejected several hundred feet in the air by the escaping gas, showing the particle-ejecting capabilities of these gases during their venting phase even for such a large scaled depth of burst. Combining these individual contributions to the crater depth gives the heavy line shown in Fig. 25.

If we make the assumption that the principal difference between impact craters and explosion craters is the effect of gas acceleration, we should eliminate this contribution and draw the picture shown in Fig. 26. Thus for surface and shallow depths of burst the craters should be quite similar, but for depths somewhat deeper than Teapot ESS, for example, one would expect serious differences to appear. However, most impact explosions are equivalent to surface or shallow-depth explosions, so one would expect relatively good agreement with existing experimental data. For a set of conditions that would result in a deeper equivalent depth of burst for an impact explosion, one would expect the above-indicated types of deviations to occur.

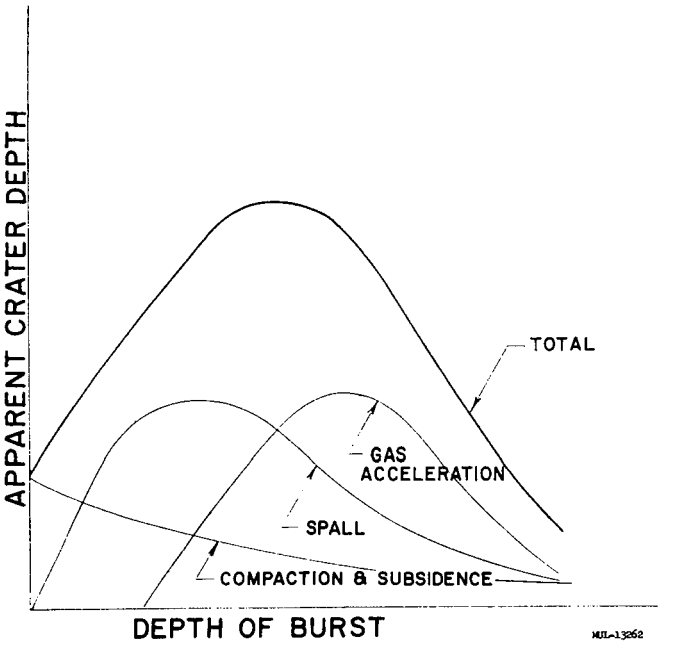

Fig. 25. Relative contributions of various mechanisms to apparent crater depth for explosion crater.

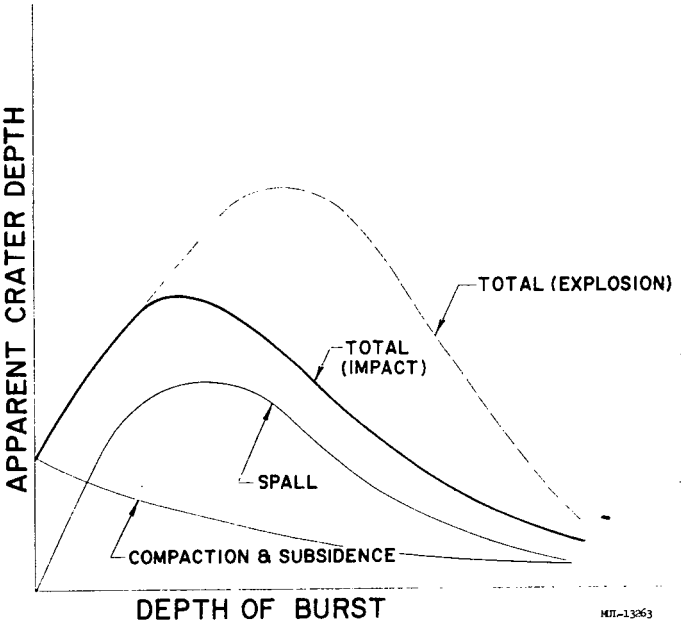

Fig. 26. Relative contributions of various mechanisms to apparent crater depth for impact crater.

A similar set of curves could be drawn for apparent crater radius, but it is very difficult to untangle the various effects. For surface detonations, spalling undoubtedly contributes to the radius to some extent. Gas acceleration is probably less important at all depths of burst in determining the radius than in determining the depth.

Conclusion

This discussion has been largely qualitative in nature, but I believe the model outlined is basically correct. Further development of this theory will require additional theoretical work as well as more experimental studies. The UNEC code has the limitation of being one-dimensional. This means that it is valid only in the vertical direction and only until such time as the rarefaction arrives back at the cavity. Work is presently being done on a two-dimensional version of UNEC which will be much more useful for cratering purposes. This code will allow much more accurate calculation of the true crater and give initial spall velocities for all the material that is ejected into the air, and should adequately treat the early stages of the gas acceleration. Calculational treatment of the late stages, when venting occurs, is impossible with present codes. Attempts are being made to develop a treatment that will handle this problem. Further experimental work directed toward exploring existing craters such as Scooter, the three Stagecoach craters, and the three large Buckboard craters should be undertaken. Geologic mapping of craters has proved invaluable in analyzing the mechanics of cratering in the past and will be even more useful in the future as we gain experience with it.

We are on the edge of constructing a quantitative picture of cratering, and are hopeful that future experimental and theoretical programs will allow the construction of a complete theory for the mechanism of explosive crater formation.

This work was done under the auspices of the U. S. Atomic Energy Commission.

REFERENCES

1. W. I. Duvall and T. C. Atchison, "Rock Breakage by Explosives," U. S. Bur. Mines, Rep. Invest. 5356 (1957).

2. A. C. Charters, "High-Speed Impact," Sci. American, pp. 128-140 (Oct., 1960).

3. R. B. Baldwin, The Face of the Moon (Univ. of Chicago Press, Chicago, 1949).

4. J. J. Gilvarry and J. E. Hill, "The Impact Theory of the Origin of Lunar Craters," Publs. Astron. Soc. Pacific, 68, 223-229 (1956).

5. E. M. Shoemaker, "Impact Mechanics at Meteor Crater, Arizona," Open file report, U. S. Geol. Survey (July, 1959).

6. G. W. Johnson, "The Soviet Program for Industrial Application of Explosions," Lawrence Radiation Laboratory, UCRL-5932 (March, 1960).

7. M. M. Dokuchaev and A. I. Kobzev, "Constructing Dams by Direct Blasting," New Technology and Pioneering Experimentation in the Construction Industry, Vol. 20, No. 9, pp. 15-17 (September, 1958) (Translation by M. I. Weinreich, Sandia Corporation, SCL-T-278, April, 1960.)

8. C. H. Noren, "The Ripple Rock Blast," Fourth Annual Symposium on Mining Research, Missouri Univ., School Mines and Met. Bull., Tech. Ser. 97, pp. 3-15 (1959).

9. J. W. Berg, Jr., "Ground Motion Measurements, New Quarry Blasts at Promontory Point, Utah," Seismol. Soc. Am. Bull. 49, No. 4, 391-397 (Oct., 1959).

10. R. H. Carlson, "High Explosive Ditching from Linear Charges," Sandia Corporation, SC-4483(RR) (April, 1961).

11. L. J. Vortman, et al., "Project Buckboard, Interim Report," Sandia Corporation, SC-4486(RR) (Nov., 1960).

12. R. E. Batzel, "Distribution of Radioactivity from a Nuclear Excavation," Lawrence Radiation Laboratory, UCRL-6249-T (Oct., 1960).

13. G. H. Higgins, "Evaluation of the Ground Water Contamination Hazard from Underground Nuclear Explosion," J. Geophys. Research 64, 1509-19 (1959).

14. L. I. Sedov, Similarity and Dimensional Methods in Mechanics (Academic Press, New York, 1959), p. 251 ff.

15. R. B. Vaile, "Pacific Craters and Scaling Laws," J. Geophys. Research 66 (Oct., 1961).

16. A. J. Chabai, "Crater Scaling Laws for Desert Alluvium," Sandia Corporation, SC-4291(RR) (Dec., 1959).

17. G. I. Pokrovskii and I. S. Fedorov, Effect of Shock and Explosion on Deformable Media (Gos. Izd., Moscow, 1957).

18. J. G. Lewis, "Crater Measurements, Operation Teapot," Engineering Research and Development Laboratory, WT-1105 (July, 1958).

19. A. V. Shelton, M. D. Nordyke, and R. H. Goeckermann, "The Neptune Event," Lawrence Radiation Laboratory, UCRL-5766 (April, 1960).

20. T. L. Thompson and J. B. Misz, "Geologic Studies of Underground Nuclear Explosions Rainier and Neptune, Final Report," Lawrence Radiation Laboratory, UCRL-5757 (Oct., 1959).

21. G. W. Johnson, G. H. Higgins, and C. E. Violet, "Underground Nuclear Detonations," J. Geophys. Research 64, 1457-1470 (1959).

22. A. V. Shelton, Lawrence Radiation Laboratory, Report to be published.

23. C. W. Lampson, "Final Report on Effects of Underground Explosions," OSRD Report 6645 (March, 1946).

24. "Crater Tests in Basalt," Isthmian Canal Studies Memo 284-P, Diablo Heights, Canal Zone (April 26, 1948).

25. "Crater Tests in Gatun Sandstone," Isthmian Canal Studies Memo 285-P, Diablo Heights, Canal Zone (May 14, 1948).

26. "Crater Tests in Residual Clay," Isthmian Canal Studies Memo 287-P, Diablo Heights, Canal Zone (May 18, 1948).

27. "Crater Tests in Marine Muck," Isthmian Canal Studies Memo 286-P, Diablo Heights, Canal Zone (May 6, 1948).

28. "Crater Tests in Cucaracha and Culebra Formations," Isthmian Canal Studies Memo 283-P, Diablo Heights, Canal Zone (April 30, 1948).

29. "Compendium of Crater Data," Waterways Experiment Station, Technical Report No. 2-547 (May, 1960).

30. E. B. Doll and V. Salmon, "Scaled HE Tests, Operation Jangle," WT-350 (Nov., 1951).

31. D. C. Sachs and L. M. Swift, "Small Explosion Tests, Project Mole, Final Report," Stanford Research Institute, AFSWP-291 (Dec., 1955).

32. "Industrial Uses of Nuclear Explosives, Plowshare," Lawrence Radiation Laboratory, UCRL-5253 (Sept., 1958).

33. B. F. Murphey, "High Explosive Crater Studies: Desert Alluvium," Sandia Corporation, SC-4614(RR) (May, 1961).

34. A. J. Chabai and L. J. Vortman, "Project Stagecoach, Interim Report," Sandia Corporation, SCTM-181-60 (1951).

35. L. J. Vortman, Sandia Corporation, private communication.

36. G. Maenchen and J. H. Nuckolls, "Calculation of Underground Explosions," Paper J, Proceedings of Lawrence Radiation Laboratory Geophysical Laboratory Cratering Symposium. Lawrence Radiation Laboratory, UCRL-6438 (Sept., 1961).

37. S. A. Feigenbaum and P. L. Wegkamp, "Photographic Earth Motion Study, Scooter Event, Final Report," Edgerton, Germeshausen & Grier, Inc., Report No. L-510 (Feb., 1961).

38. H. Jones and A. R. Miller, "The Detonation of Solid Explosions," Proc. Roy. Soc. (London) A194, 480-507 (1948).

39. D. L. Martin and W. J. Hinge, "Energy Partition of Underground Explosions," Engineering Research and Development Laboratories, AFSWP-789 (March, 1958).

40. R. H. Morris and R. C. Schneiderhan, "Earth Motion Studies, Operation Hardtack, Phase II," Edgerton, Germeshausen & Grier, Inc. ITS-1706 (Feb., 1959).

jd

APPENDIX A

I would like to express my gratitude to Sandia Corporation personnel who compiled the following data on crater dimensions. In many cases, original drawings were consulted to resolve uncertainties. This is believed to be the best data available at the present time. The programs are listed in chronological order and the shots within each program are ordered by increasing depth of burst.

Series Name	Shot Designation	Charge Weight (lb)	Depth of Burst Z(ft)	Apparent Crater Radius R(ft)	Apparent Crater Radius D(ft)	Apparent Crater Volume $V(ft^3)$
Jangle H. E.	HE-4	2560	-2.05	6.90	1.90	110
	HE-1	2560	2.05	18.50	6.70	2010
	HE-7	2560	2.60	19.00	6.70	3300
	HE-6	2560	3.01	19.80	6.10	3600
	HE-5	2560	4.10	19.40	7.50	4000
	HE-3	2560	6.84	20.27	10.80	6000
	HE-2	40,000	5.13	39.00	15.00	35,000
	HE-9*	216	0.84	8.30	3.50	270
	HE-10*	216	3.00	11.30	5.50	860
Mole	207	256	-0.83	4.05	1.40	37
	206	256	0.00	6.35	1.70	129
	205	256	0.83	8.90	2.20	312
	204	256	1.65	9.45	2.40	364
	203	256	3.17	8.35	4.10	358
	202	256	6.35	11.40	5.90	1027
	212	256	6.35	11.20	6.07	1174
ERDL	403	256	0.83	8.36	3.37	301
	405	256	1.65	9.24	4.60	511
	401	256	3.17	10.59	5.45	837
	406	256	3.17	9.95	4.22	686
	402	256	4.76	11.05	6.25	961
	404	256	6.35	12.10	6.12	1195

* These data were not included in the analysis presented in this report.

APPENDIX A (continued)

Series Name	Shot Designation	Charge Weight (lb)	Depth of Burst Z(ft)	Apparent Crater Radius R(ft)	Apparent Crater Radius D(ft)	Apparent Crater Volume V(ft^3)
	8	256	6.35	13.13	7.30	1489
	2	256	9.53	15.12	7.86	2146
	9	256	9.53	14.14	7.16	1930
	10	256	12.70	13.40	4.10	1093
	16	256	12.70	14.19	6.70	2220
Sandia	4	256	15.90	11.32	1.77	368
Series I	11	256	15.90	6.53	0.38	236
	12	256	19.05	9.36	2.30	256
	17	256	19.05	5.68	1.70	55
	15	256	25.40	4.18	0.45	31
	S-12	256	0.00	8.57	2.49	161
	S-13	256	0.00	8.34	2.60	267
	11	256	13.10	14.69	5.43	1670
	10	256	16.10	14.10	4.55	1077
	9	256	16.40	14.29	2.61	716
Sandia	8	256	19.00	10.07	1.60	297
Series II	7	256	19.70	8.13	1.01	121
	6	256	22.60	4.39	1.00	170
	5	256	23.30	3.03	0.30	18
	4	256	25.50	2.35	1.15	16
	3*	256	26.10	32.30	-1.03	-584
	2*	256	28.50	37.70	-0.83	-1079
	1*	256	29.80	31.00	-0.63	-1187
	2	40,000	17.1	50.5	23.6	83,650
Stagecoach	3	40,000	34.2	58.6	29.2	144,600
	1	40,000	80.0	57.0	7.9	49,145
Scooter		1,000,000	125.0	153.8	74.5	2,642,000

* These shots resulted in mounds instead of craters and have been included in this summary for completeness. However, these data have not been used in the analysis.

LIST OF PREVIOUS PLOWSHARE AND/OR RELATED REPORTS

Report No.	Title
UCRL-4659	Deep Underground Test Shots.
UCRL-5026	Non-Military Uses of Nuclear Explosions.
UCRL-5124 Rev. I	Phenomenology of Contained Nuclear Explosions.
UCRL-5253	Industrial Uses of Nuclear Explosives.
UCRL-5257 Rev.	Peaceful Uses of Fusion.
UCRL-5281	Temperatures and Pressures Associated with the Cavity Produced by the Rainier Event.
UCRL-5457	Large Scale Excavation with Nuclear Explosives.
UCRL-5458	Mineral Resource Development by the Use of Nuclear Explosives.
UCRL-5538	Evaluation of the Ground Water Contamination Hazard from Underground Nuclear Explosions.
UCRL-5542 Rev.	Properties of the Environment of Underground Nuclear Detonations at Nevada Test Site. Rainier Event.
UCRL-5623	Radioactivity Associated with Underground Nuclear Explosions.
UCRL-5626	Underground Nuclear Detonations.
UCRL-5709	Hydroclimatology and Surface Hydrology of San Clemente Island.
UCRL-5757	Geologic Studies of Underground Nuclear Explosions Rainier and Neptune.
UCRL-5766	The Neptune Event. A Nuclear Explosive Cratering Experiment.
UCRL-5840	Industrial and Scientific Applications of Nuclear Explosions.
UCRL-5882 Rev.	Chemical Reactions Induced by Underground Nuclear Explosions.
UCRL-5917	Excavation with Nuclear Explosives.
UCRL-5928	Nuclear Explosives and Mining Costs.
UCRL-5932	The Soviet Program for Industrial Applications of Explosions.

Report No.	Title
UCRL-5949	An Application of Nuclear Explosives to Block Caving Mining.
UCRL-5968	An In Vacuo Electromagnetic Dispersion Experiment.
UCRL-6008	Some Potential Uses of Nuclear Explosives in the Conservation and Development of Water Resources.
UCRL-6013	Probing the Earth with Nuclear Explosions.
UCRL-6030-T	Application of Nuclear Explosions as Seismic Sources.
UCRL-6054	Fracturing of Rock Salt by a Contained High Explosive.
UCRL-6175	The System H_2O-NaCl at Elevated Temperatures and Pressures.
UCRL-6215	Can Peaceful Nuclear Explosions be Conducted Safely?
UCRL-6240	Cavity Definition, Radiation and Temperature Distributions Resulting from the Logan Event.
UCRL-6249-T	Distribution of Radioactivity from a Nuclear Excavation.
UCRL-6251	Radiation and Temperature Measurements of the Neptune Event.
UCRL-6274	Final Report on the Pinot Experiment.
UCRL-6311	The Hugoniot Equation of State of Rocks.
UCRL-6374	Results and Power Generation Implications from Drilling into the Kilauea Iki Lava Lake, Hawaii.
UCRL-6578	On Cratering. A Brief History, Analysis, and Theory of Cratering.

* * *

Plowshare Series: Report No. 2. Proceedings of the Second Plowshare Symposium (Held at San Francisco, May 13 - 15, 1959):

UCRL-5675	Part I: Phenomenology of Underground Nuclear Explosions.
UCRL-5676	Part II: Excavation.
UCRL-5677	Part III: Recovery of Power and Isotopes from Contained Underground Nuclear Explosions.
UCRL-5678	Part IV: Industrial Uses of Nuclear Explosives in the Fields of Water Resources, Mining, Chemical Production, and Petroleum Recovery.
UCRL-5679	Part V: Scientific Applications of Nuclear Explosives in the Fields of Nuclear Physics, Seismology, Meteorology and Space.